Graduate School ETD Form 9
(Revised 12/07)

PURDUE UNIVERSITY
GRADUATE SCHOOL
Thesis/Dissertation Acceptance

This is to certify that the thesis/dissertation prepared

By Renxiang Wang

Entitled
Lithium Ion Battery Failure Detection Using Temperature Difference Between Internal Point and Surface

For the degree of Master of Science in Electrical and Computer Engineering

Is approved by the final examining committee:

Yaobin Chen
Chair

Rongrong Chen

Maher Rizkalla

To the best of my knowledge and as understood by the student in the *Research Integrity and Copyright Disclaimer (Graduate School Form 20)*, this thesis/dissertation adheres to the provisions of Purdue University's "Policy on Integrity in Research" and the use of copyrighted material.

Approved by Major Professor(s): Yaobin Chen

Approved by: Yaobin Chen 12/01/2011
Head of the Graduate Program Date

Graduate School Form 20
(Revised 9/10)

PURDUE UNIVERSITY
GRADUATE SCHOOL

Research Integrity and Copyright Disclaimer

Title of Thesis/Dissertation:

Lithium Ion Battery Failure Detection Using Temperature Difference Between Internal Point and Surface

For the degree of Master of Science in Electrical and Computer Engineering

I certify that in the preparation of this thesis, I have observed the provisions of *Purdue University Executive Memorandum No. C-22,* September 6, 1991, *Policy on Integrity in Research.**

Further, I certify that this work is free of plagiarism and all materials appearing in this thesis/dissertation have been properly quoted and attributed.

I certify that all copyrighted material incorporated into this thesis/dissertation is in compliance with the United States' copyright law and that I have received written permission from the copyright owners for my use of their work, which is beyond the scope of the law. I agree to indemnify and save harmless Purdue University from any and all claims that may be asserted or that may arise from any copyright violation.

Renxiang Wang

Printed Name and Signature of Candidate

12/01/2011

Date (month/day/year)

*Located at http://www.purdue.edu/policies/pages/teach_res_outreach/c_22.html

LITHIUM ION BATTERY FAILURE DETECTION USING TEMPERATURE DIFFERENCE BETWEEN INTERNAL POINT AND SURFACE

A Thesis

Submitted to the Faculty

of

Purdue University

by

Renxiang Wang

In Partial Fulfillment of the

Requirements for the Degree

of

Master of Science in Electrical and Computer Engineering

December 2011

Purdue University

Indianapolis, Indiana

To my family.

ACKNOWLEDGMENTS

First of all, I am extremely grateful to my wife Qingmin Xu, my son Albert Wang and my daughter Kelly Wang who have been instrumental in my achievements. Their unflinching support has allowed me to further my research and studies. I would also like to thank them for their encouragement. I sincerely thank Dr. Yaobin Chen, my adviser, for the majority of my education in completing my M.S. studies. To Dr. Chen, my experiences in doing research with you on the Lithium Battery Catastrophic Failure Early Detection project, your control theory class, and constant guidance throughout my difficulties in both my study and research work, I give to you my heartfelt thanks and appreciation. I would like to thank Dr. Rongrong Chen who has guided me in the initial phases of my research work. I am grateful to her for supporting my experiments in my thesis work. She has always inspired me as a teacher and a researcher. She has provided me timely guidance in learning the fundamentals of battery and renewable energy theory. I would like to thank Professor Jian Xie who has guided me in the final phase of my research work. He has provided a good support system for me academically remove the coma in the area of lithium ion batteries. I also thank him for the knowledge he has shared from his group meetings. I would like to thank the Naval Surface Warfare Center Crane Division, in providing me an opportunity to work on the Lithium Battery Catastrophic Failure Early Detection project. My learning experiences in tackling the challenges of this project, and the organizing and documentation of a large project. I would like to give my sincere thanks to Crane for the sponsoring of my thesis study. I express my sincere gratitude to my classmates Yao Zhai, Jie Xue, Meng Wu, Hui He and Yaodong Liu and my research cooperator Hao He. All of whom were with me through my difficult situation academically. I also thank other friends for their friendship which I would cherish forever. Especially, I would like to express my gratitude to Dr. Jin Wang who has

been my adviser at Ohio State University. Dr. Jin Wang initiated my study and career in the research of power electronics and batteries and let me do instrumental work for his projects. I would like to thank him for his support in my job seeking as well.

TABLE OF CONTENTS

Page

Page

LIST OF TABLES

LIST OF FIGURES

ABSTRACT

Wang, Rengxiang. M.S.E.C.E, Purdue University, December 2011. Lithium ion Battery Failure Detection Using Temperature Difference Between Internal Point And Surface. Major Professor: Yaobin Chen.

Lithium-ion batteries are widely used for portable electronics due to high energy density, mature processing technology and reduced cost. However, their applications are somewhat limited by safety concerns. The lithium-ion battery users will take risks in burn or explosion which results from some internal components failure. So, a practical method is required urgently to find out the failures in early time. In this thesis, a new method based on temperature difference between internal point and surface (TDIS) of the battery is developed to detect the thermal failure especially the thermal runaway in early time. A lumped simple thermal model of a lithium-ion battery is developed based on TDIS. Heat transfer coefficients and heat capacity are determined from simultaneous measurements of the surface temperature and the internal temperature in cyclic constant current charging/discharging test. A look-up table of heating power in lithium ion battery is developed based on the lumped model and cyclic charging/discharging experimental results in normal operating condition. A failure detector is also built based on TDIS and reference heating power curve from the look-up table to detect aberrant heating power and bad parameters in transfer function of the lumped model. The TDIS method and TDIS detector is validated to be effective in thermal runaway detection in a thermal runway experiment. In the validation of thermal runway test, the system can find the abnormal heat generation before thermal runaway happens by detecting both abnormal heating power generation and parameter change in transfer function of thermal model of lithium ion batteries. The result of validation is compatible with the expectation of detec-

tor design. A simple and applicable detector is developed for lithium ion battery catastrophic failure detection.

1. INTRODUCTION

1.1 Overview

Lithium-ion battery has become a popular power source for consumer electronics, portable devices and hybrid vehicles due to the high energy density, high power density and low pollution in recent decades. The rapid increasing hybrid vehicle market boosts the huge demand of lithium-ion batteries as well. Lithium-ion battery also plays more and more important roles in energy storage system for renewable energy harvesting as an important member of secondary batteries. Basically, as other secondary batteries, lithium-ion batteries (LIB) is a family of rechargeable batteries which can provide two functions to provide electric power supply and to store energy in electro-chemistry. The two functions are generally called the process of charging and discharging respectively. Because of the unsafely nature, the lithium-ion batteries have risk to burn or to explode to result in catastrophic aftermath. Among the factors to lead a lithium-ion battery to abuse, the temperature plays a key role in the abuse progress. Therefore, the thermal behaviors are more and more important to be studied in lithium-ion battery the battery failure which can be described by abnormal thermal behavior should be detected by the aberrant temperature change in LIB. In this thesis, a method will be developed to detect abnormal temperature behavior in LIB based on the detection of temperature deference between internal point and surface.

1.2 History of Lithium-ion Batteries

The first battery is generally called Volta cell. It was invented in 1800 by an Italian physicist Alessandro Volta. After that, the commercialization and technology

of batteries were developed rapidly. A huge industry and market was formed after that. However, it is interesting that only three types of batteries, include MnO_2 primary cell, Lead acid secondary cell and nickel based secondary have been widely used although a large number of different batteries were invented or developed in the last century. Nowadays, with the development of electronics and hybrid vehicles, the batteries are required to have better performance and abilities. The old batteries cannot catch up with high-end application due to the technical limits. The lithium-ion battery was invented in responding to the demand of high performance batteries.

The development of lithium ion battery based on the physical nature of lithium metal. The Li metal is the lightest element in metals. Therefore, lithium metal as anode has more energy density than other anodes. However, lithium metal easily reacts with water and generates hydrogen gas. Therefore the aqueous electrolyte cannot be applied with lithium metal. It increases the difficulty and risk in developing practical rechargeable lithium batteries. Lithium metal anode primary batteries based on non-aqueous electrolytes like propylene carbonate-lithium perchlorate and lithium negative electrodes were developed in the early 1970's.

With removing roadblocks of technology in non-aqueous electrolyte, the lithium-ion batteries were first proposed by M. Stanley Whittingham at Binghamton University, at Exxon in 1970s [1]. Whittingham made the lithium-ion battery with a titanium sulfide cathode and a lithium metal anode. To improve the safety of lithium-ion batteries, the electrochemical properties of lithium intercalation in graphite were first invented in 1980 by Rachid Yazami et al., at the Grenoble Institute of Technology (INPG) and French National Center for Scientific Research (CNRS) in France. They showed the reversible intercalation of lithium into graphite in a lithium/polymer electrolyte/graphite half cell. Their work was published in 1982 and 1983 [2] [3]. Both of thermodynamics and kinetics of the batteries were shown in good reversibility. After this half cell lithium-ion battery was validated. In 1981, Bell Labs developed a workable graphite anode to provide an alternative to the lithium metal battery in which

both anode and cathodes are made of a material containing lithium ions. Also, John Goodenough and his group did groundbreaking research on cathode materials [4].

In 1983, a cathode material with Spinel crystal structure was developed by Michael Thackeray, Goodenough, and coworkers [5]. This Manganese Spinel (LMO) cathode material shows some advantages, such as low cost, good electronic, good lithium ion conductivity and good structural stability due to its three-dimensional structure. A flaw of the manganese based cathode is that the Spinel can be faded by cyclic aging. But, this drawback can be overcome with chemical modification of the material [6]. The Manganese spinel has already be applied in commercial cells now [7].

Another progress was made in 1989. The lithium-ion battery can generate higher voltage if the cathode is coated by polyanions, e.g. sulfates. The increased voltage results from the inductive effect of polyanion. Goodenough and Arumugam Manthiram of the University of Texas at Austin discovered the effect of polyanion which is coated on cathodes [8].

In 1996, the lithium iron phosphate ($LiFePO_4$) and other phospho-olivines (lithium metal phosphates with olivine structure) material were discovered and identified as cathode materials by Goodenough, Akshaya Padhi and coworkers [9].

In 2002, Yet-Ming Chiang and his group at MIT found that the material's conductivity can be improved by doping with aluminum, niobium and zirconium. Although the mechanism of doping effect has not been clear yet, this topic reignited a heated debate [10].

In 2004, Yet-Ming Chiang again increased performance by utilizing iron-phosphate nano-particles with size less than 100 nanometers in diameter. The nano size particles can much increase the cathode surface area to overcome the low conductivity of lithium iron phosphate material. This technology can improve the capacity and performance of lithium-ion batteries greatly. From then on, a competition in commercialization and patent between Chiang and Goodenough was triggered [11].

In the meantime, the commercialization of lithium-ion battery has been preceded. The first commercial lithium-ion battery was developed in Japan by Asahi Kasei

Co [12]. and first commercialized by Sony Company in 1991 [13]. And then, the A&T Battery Company, a joint company of Toshiba Battery and Asahi Kasei Co. started mass-production of lithium-ion batteries in 1992. This new battery was welcome and accepted in market immediately since its high energy density, low loss of charge and no memory and lazy effects as occurred with nickel-cadmium (Ni-Cd) and nickel-metal hydride (Ni-MH) batteries. In addition, the environmental hazard of lithium-ion battery is much less than Ni-Cd battery and Lead/Acid battery which can cause substantial pollution of heavy metal. Since then, the capacity of commercial lithium-ion batteries has much improved through engineering and the introduction of graphite anodes, improved $LicoO_2$ based cathode materials, and the introduction of electrolyte additives. In 1998, Ube Industries Ltd. introduced a high-purity "functional electrolyte" which contained special additives that reacted during the first charging to form solid electrolyte interphase SEI which can prevent electrolyte decomposition [14] [15]. As a result, the capacity of anode carbon material increased up to 320 mAh/g. It is approaching to the theoretical value 372 mAh/g. In 2003, the Ube has developed other new additives to eliminate electrolyte decomposition of active spot on cathode [16] [17]. Just as his previous additives on anode, Ube expanded the SEI additives to effect on cathode material. With the commercialization and development of lithium-ion batteries and related materials, the capacity of commercial lithium-ion battery increases and gradually approaches to theoretical capacity. For example, the capacity of a cylindrical 18650 cell increased from early 800 mAh to 2.9 Ah by 2006 after the commercialization of lithium-ion battery started in 1992.

In recent years, researchers have made big progresses in Cathode, Anode and new type of Electrode. A variety of new technologies improved the lithium-ion battery in energy density, power density durability, safety, manufacturing process and cost.

With respect to the cathode of LIB, the lithium ion fluorine phosphate was developed in 2007 by University of Waterloo to improve the durability and decrease the cost because the Li element can be replaced by cheaper Na metal or Na/Li alloy [18]. In 2008, to improve the safety of $LiCoO_2$, the Lithium nickel manganese

cobalt (NMC) material was applied to the cathode of LIB by Imara Corporation [19]. In the same year, 5% Vanadium-doped Lithium iron phosphate olivine was used as cathode material by Binghamton University to increase the output power of LIB [20]. In 2009, engineers at the University of Dayton Research Institute developed the first solid-state, rechargeable lithium-air battery which gives a solution of high energy density and safety of LIB in another way [21]. In the meantime, some breakthrough results were obtained in the study of anode material of LIB. In 2006, Ki Tae Nam, Dong-Wan Kim at MIT developed virus synthesis and assemble of nanowires for anode of LIB [22]. Yi Cui and his group at Stanford University used nano-sized silicon wires on stainless steel instead of regular graphite anode to get high capacity of LIB in 2007 [23].

Up to date, new materials and technologies for LIB are still being discovered to catch up with the increasing demand for high performance batteries, power supplies and energy storage. Furthermore, the demand for cleaner environment and more efficient energy products will continue to motivate researchers and engineers to develop advanced and reliable lithium-ion batteries for broad applications.

1.3 Structure and Chemistry of Lithium-ion Batteries

An electrical battery is a device which can convert chemical energy to electrical energy. A battery consists of the positive electrode, the negative electrode and electrolyte [24]. There are two types of electrical batteries: primary batteries (disposable batteries), which can be only used once, and secondary batteries (rechargeable batteries), which can be used multiple times by recharging. The lithium-ion battery is a secondary battery.

A typical lithium-ion battery has five components - the cathode (Positive), the anode (Negative), the electrolyte, the separator and the package. Figure 1.1 shows the structure in a prismatic type of lithium-ion battery. In this battery, the positive electrode and negative electrode are separated by separator. The separator is soaked

with non-aqueous electrolyte to connect the two electrodes. The negative and positive terminals are set on the case of battery to connect the lithium-ion cell to outside electrical circuit. An important function of the case or package is to isolate the internal cell to water or moisture. The lithium-ion battery is very sensitive to water which can react to lithium metal or breakdown electrolyte. The good seal of case may prolong the life of battery. Besides, the gas release vent also is designed in a case to prevent the battery from exploding because of high internal gas pressure.

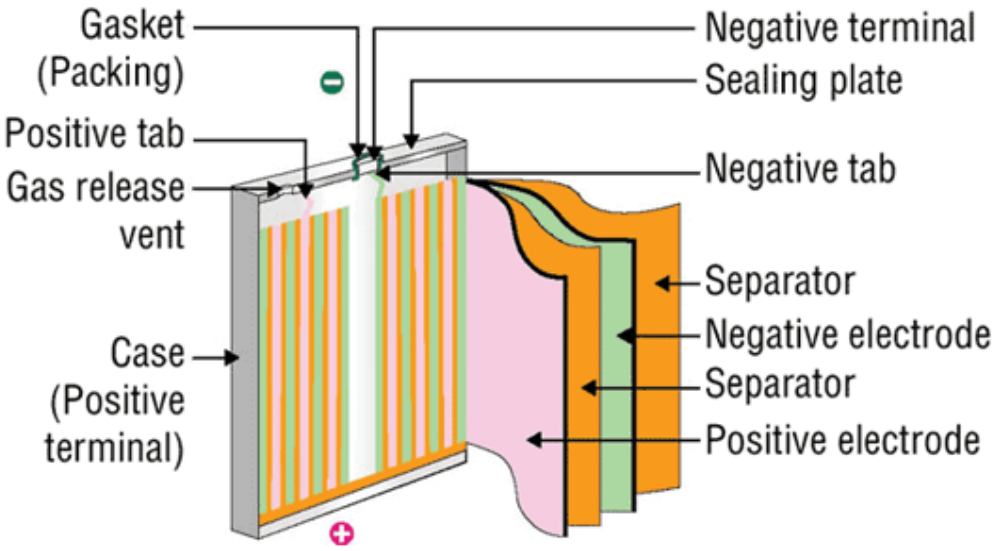

Fig. 1.1. Lithium-ion battery structure

In the battery, three functional components related to electrochemical reaction directly. They are the cathode, the anode and the electrolyte. The cathode contains some active material, such as $LicoO_2$, $LiMn_2O_4$, $LiNiO_2$, $LiFePO_4$, $LiCo_{1/3}Ni_{1/3}Mn_{1/3}O$, $Li(Li_aNi_xMn_yCo_z)O_2$ and so on. In the anode, the material includes Graphite ($LiPF_6$), hard carbon, $Li_4Ti_5O_{12}$, Si, Ge, etc. Liquid electrolytes in lithium-ion batteries consist of lithium salts, such as $LiPF_6$, $LiBF_4$ or $LiClO_4$ in an organic solvent, such as ethylene carbonate, dimethyl carbonate, and diethyl carbonate.

As a rechargeable battery, the lithium-ion battery can work in charging and discharging process. In charging process, as shown in Figure 1.2, the lithium-ions are

migrated through electrolyte and insert to anode. The electrical energy is stored in chemical form. During the discharging process, as shown in Figure 1.3, the lithium ions are extracted from anode and moved to the cathode. The electrons flow over the outside load to generate electrical power.

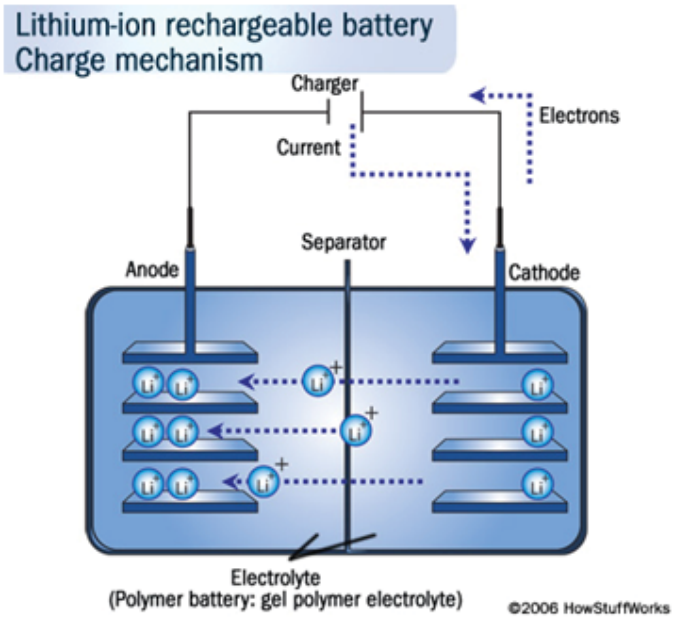

Fig. 1.2. The charging process in a lithium-ion battery

Normally, the electrochemical reaction in a LIB is reversible. Take $LiCoO_2$ LIB for an example. In the cathode part, the electrochemical reaction is:

$$LiCoO_2 \rightleftarrows Li_{1-x}CoO_2 + xLi^+ + xe^- \tag{1.1}$$

The corresponding electrochemical reaction on anode is:

$$xLi^+ + xe^- + 6C \rightleftarrows Li_xC_6 \tag{1.2}$$

In some cases, the reversibility of charging/discharging maybe destroyed to reduce the life of LIB. For example, if a LIB is over-discharged, the reaction on cathode should be:

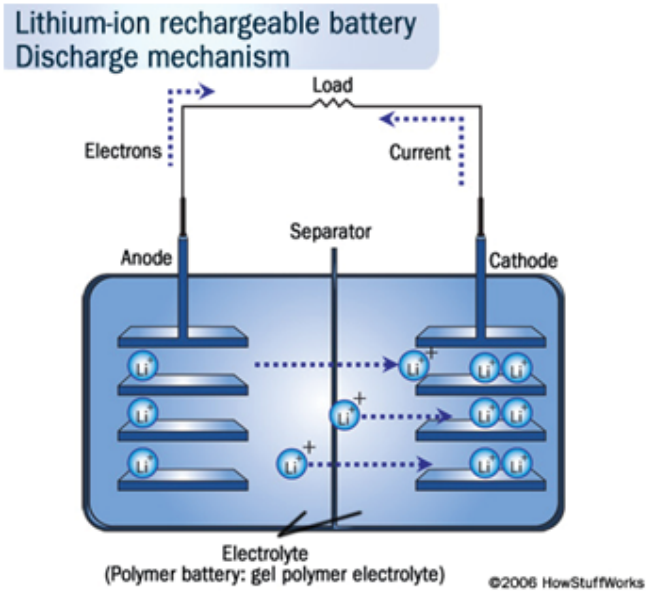

Fig. 1.3. The discharging process in a lithium-ion battery

$$Li^+ + LiCoO_2 \rightarrow Li_2O + CoO \tag{1.3}$$

In this reaction, the lithium cobalt oxide cannot be decomposed to lithium-ions. This irreversible reaction can result in defective cathode materials to shorten the life of the battery [25].

If the LIB is over-charged, the following reaction may happen on the cathode.

$$LiCoO_2 \rightarrow Li^+ + CoO_2 \tag{1.4}$$

This irreversible reaction can also defect the active material on cathode to reduce the life of the LIB [26]. Moreover, the high valence ion on cathode probably brings on the risk of exploding. In addition, the over-discharge and over-charge can generate a large amount of heat which may result in thermal runway in LIB potentially.

In actual application, the lithium-ion batteries are used as a battery pack. Especially in HEV or electric vehicle, to increase the power of batteries, the lithium-ion batteries are connected in series or in parallel in a battery module. The modules are

packaged in a battery pack to generate enough electric power to drive motors. To manage and protect the battery module, a battery management system works with the module usually. Figure 1.4 shows the structure of a lithium-ion battery module example.

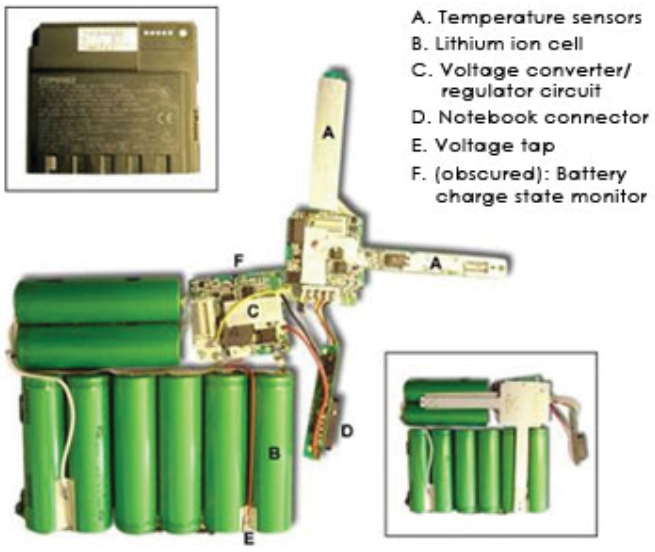

Fig. 1.4. The structure of a lithium-ion battery module

1.4 Temperature Hazard of a Lithium-ion Battery

The lithium-ion battery is temperature-dependant in voltage, power, capacity and life. In most types of lithium-ion batteries, the lithium battery should be operated within a normal operating temperature range of -10 to 60 °C. The Figure 1.5 shows the temperature effects on safety of a lithium-ion battery.

In low temperature, the electrochemical reaction goes slowly according to the Arrhenius Law. The inactive chemicals result in the slow transferring rate of ions and electrons on the electrochemical interface. The slow transfer rate leads to the reduction of current carrying capacity. So, both of the charging and discharging current is decreased in low operating temperature. It means that the power performance

of the lithium-ion battery comes worse in low temperature especially for high-power lithium-ion batteries [27]. Furthermore, at low temperature, the process of lithium-ion intercalation becomes more and more difficult. The hard intercalation makes that the lithium-ions difficult to insert into the layers of graphite on anode. The lithium metal has to deposit on the surface of anode to form lithium plating layer. This process results in irreversible capacity loss of the lithium-ion battery. Another low temperature effect is the reduction of life for lithium-ion batteries. The Figure 1.6 shows the life of LIB at different operating temperatures. If the operating temperature is lower than zero degree, the life of the battery falls down with the temperature going down.

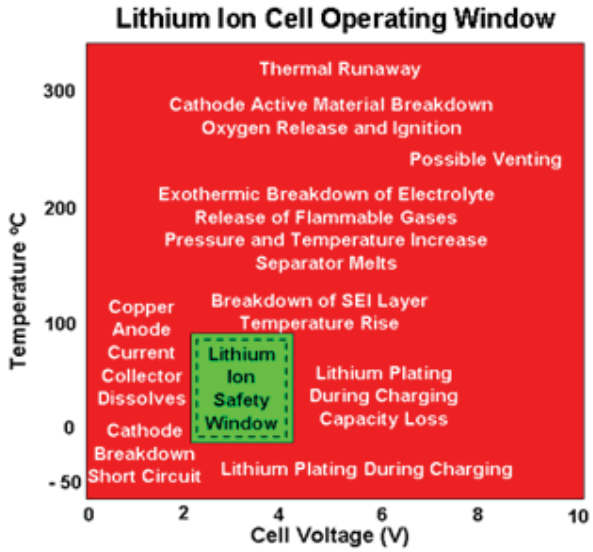

Fig. 1.5. The temperature effects on safety of a lithium-ion battery

At high temperature, the lithium-ion batteries take more risk of failure than at low temperature. Many problems which result in the destruction of the cell are caused by the high operating temperature. If the operating temperature increases from 80 °C to the temperature that can cause permanent damage of the battery, several stages are involved in devastating the lithium battery in different mechanisms. In

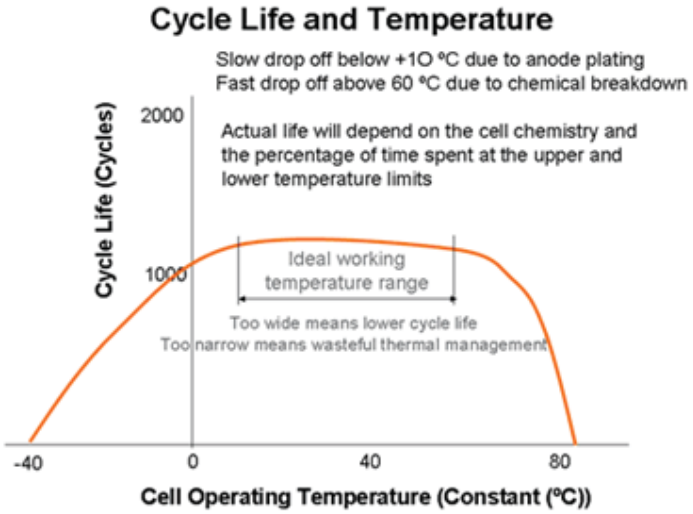

Fig. 1.6. The effects of temperature on lithium-ion batteries

the first stage the SEI layer on the anode start to breakdown due to overheating or physical penetration. The destruction of SEI may be tripped by large currents, overcharging/discharging or excessive operating temperature. Once the SEI is broken, the reaction on the interface between electrolyte and anode will be accelerated without the constraining of SEI layer. A large amount of heat is generated after SEI layer removed. In the second stage, the organic solvents in electrolyte start to breakdown and release flammable hydrocarbon gases. This stage typically starts at 70 °C to 110 °C which depends on the types of electrolyte. The gassing process causes the rise up pressure inside the battery. Normally, the gas can be released by safety vent to relieve the internal pressure. Occasionally, explosion can happen due to the rapid increasing internal pressure. If the combustible hot gas is released to air, the battery can possibly burn. The third stage begins at the temperature about 135 °C. The polymer separator starts to melt. The shirked holes shut down the tunnel of lithium-ions. The transfer of Lithium-ions between anode and cathode is stopped by melted separator. In last stage, the cathode materials breakdown happens at around 200 °C

for $LiCoO_2$ material but at higher temperatures for other cathode chemistries. The battery is permanently damaged in function and structure in this stage [28].

Thermal runaway is the worst condition in lithium-ion battery failure. When thermal runaway happens, the heating power generated by battery is much over than the dissipation of heat power. The temperature of the battery increases sharply to lead to thermal runaway. In this condition, the temperature of lithium-ion battery is out of control and results in catastrophic consequences such as burning, exploding and damage of structures. Once the thermal runaway occurs, the damaging process of batteries can possibly go through all the stages mentioned in high temperature section. The thermal runway not only damages the basic function of battery, but also goes with decomposition of electrolyte, defection of electrodes, gassing, burning even explosion in the process of temperature rising.

The Figure 1.7 shows the factors and process of thermal runaway formation.

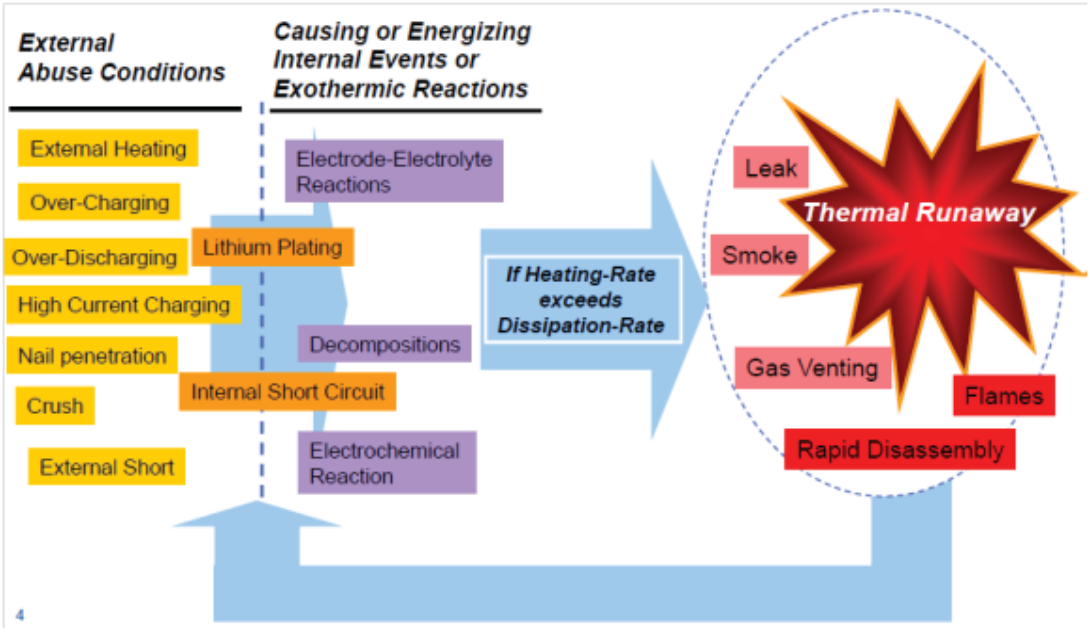

Fig. 1.7. The factors and process in thermal runaway forming

1.5 Failure Detection Methods

The safety of lithium-ion battery is a roadblock for application. In recent years, some electronic manufacturers recalled batteries which may have risks of burning or exploding. To overcome this problem, some methods were developed for protecting lithium batteries.

The failure of lithium-ion batteries is small probability event. Figure 1.6 shows the distribution of battery failures in a battery life cycle. The upper curve shows the variation of the instantaneous failure rate over time. The curve shows a "Bathtub" curve which is similar to the failure distribution curve of other electronic components. The lower curve shows that the cumulative failure distribution relative to instantaneous failure. According to Figure 1.8, in the initial period of battery life, the fatalities happen more frequently than useful life period. If some potential factors to cause failure can be found in early period, the battery may be saved from catastrophic failures.

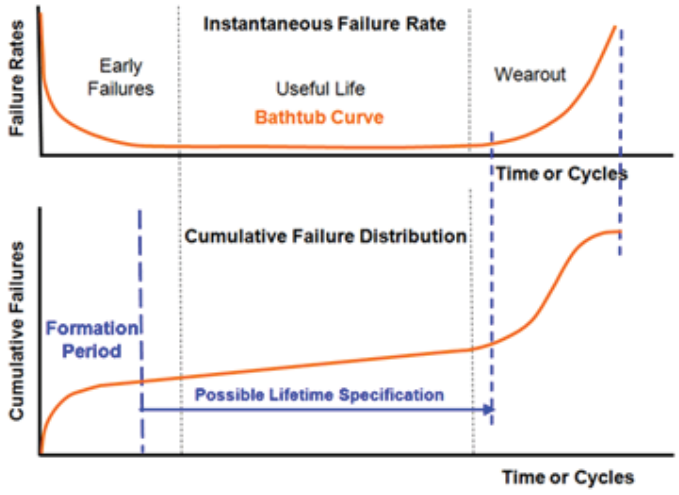

Fig. 1.8. The distribution of battery failures in a lithium-ion battery life cycle

Generally, the protection methods should protect the lithium batteries from following events or conditions:

• System isolation

- Battery abuse
- Over current
- Short circuit
- Over voltage - Over charging
- Under voltage - Over discharging
- High ambient temperature
- Overheating
- Excessive internal pressure

Except the system isolation and battery abuse, other events or conditions result from temperature directly or indirectly. Therefore, the thermal issue is an important aspect in lithium-ion battery protection.

Traditional protection methods manage or protect batteries with static parameters. Most of failure detection circuit for protective function base on the sensing of voltage, current and temperature. According to the measurement of the parameters, the protection devices will be responding to the abnormal value of voltage, current, temperature and internal pressure. For example, Figure 1.9 and Figure 1.10 show two stratagems in battery management and protection using current vs. temperature and voltage vs. temperature respectively. In both of the figures, the green area is a normal operating window which was preset to operate and control battery safely in this area. The electronic protection, resettable fuse and thermal fuse act respectively once the current, voltage or temperature goes out of the safe area.

Some safety devices are adopted to realize the protective functions, such as safety vents, thermal fuse, positive temperature coefficient element (PTC), and circuit breakers [29]. These safety devices can shut down the current once unexpected events happen and exceed the pre-set limit. Some factors will affect the operation of these devices such as the ambient temperature, thermal dynamic properties of the batteries, heating power of the batteries, cumulative heat in a battery pack, and the rate and time of charge or discharge [28].

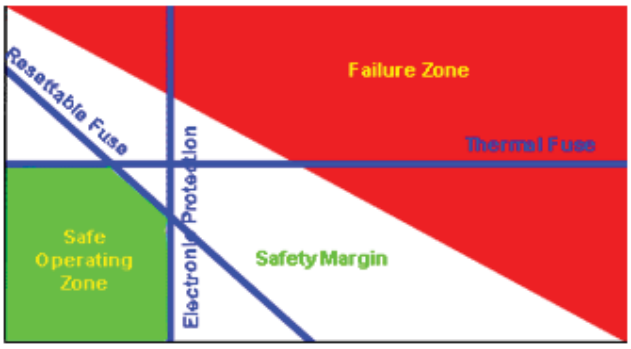

Fig. 1.9. Current based battery protection stratagem

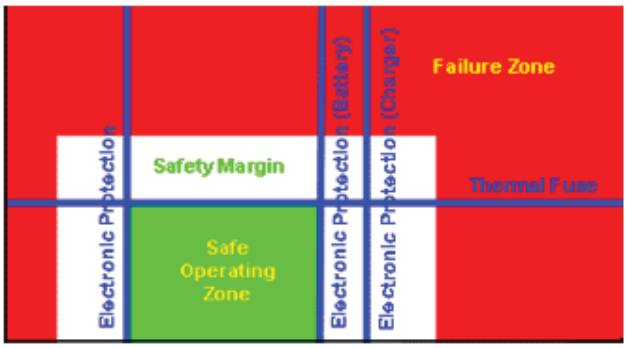

Fig. 1.10. Voltage based battery protection stratagem

Besides the safety vents, thermal fuse, PTC, and circuit breakers, some new technologies also can improve safety of lithium-ion battery in chemical stability, thermal stability and mechanical strength. An improvement of battery component is the Shutdown Separator. The Shutdown Separator has a high-density polyethylene layer which can melt down at 135°C [30]. Once shutdown happens, the Lithium-ions transportation is stopped by the melted HDPE film. The electrochemical reaction rate will be slow down due to the shutdown action. Besides the Shutdown separator, other improvements such as non-flammable electrolytes, redox shuttles, shutdown additives, electrolyte salts, active materials and coatings were made to enhance the safety of lithium-ion battery in battery structure and chemical materials [31] [32] [33] [34] [35].

Normally, a Battery Management System (BMS) is responsible to manage and protect lithium-ion batteries in a Battery module. The Electronic safety circuits are part of the BMS to detect failure and to protect the battery using current, voltage and temperature signals. This part of BMS commonly called protection circuit module (PCM). The PCM are usually attached to battery packs as separate modules. In the event of an abnormal condition, such as short circuit, over charge, over discharge and over temperature, the PCM closes the wrong battery off the packs. The packs are protected from damaging in the wrongful condition. Some system can record the abnormal events as a profile of battery to identify the safety level in diagnostic system [36].

Catastrophic failure may be due to the short circuits resulting from contaminated materials, mechanical tolerance problems, burrs, dendrites, and lithium plating. The broken welds, loose connections, or cracks, external faults such by Battery management failures can also cause failures in the cells should be protected. Therefore, if the failures can be found in early time, the system of pack management will have enough time to take protective action to save the whole pack from severe failures. Some researchers tried to use different methods to assess or detect failure of lithium-ion batteries.

Mikolajczak, C.J. et al. tried to use a scientific methodology to build an expertise system to gather the information for the process in which the lithium-ion battery goes to failure gradually [37]. The information includes the life of the battery, state of the system at the time of incident, usage environment, extenuating factors and user's actions in response to the incident. The investigation will be used to assess the state of health so as to predict the failure of the lithium ion batteries.

J. Loud, et al. investigated the factors cause catastrophic failure in the lithium ion batteries by use experimental methods [38]. Loud simulated the internal short circuit by employing nail test for studying cell responses to internal failure. The test data for this test can also be used for predicting catastrophic failure in lithium ion batteries.

U. Troltzsch, et al. use impedance spectroscopy to characterize the aging effects in lithium ion batteries [39]. The probability of failure increases with the age of a lithium battery. In other words, the failure of lithium ion batteries is the accumulation of aging factors. Troltzsch measured the impedance of lithium ion batteries to rate the state of life and state of health of battery. Therefore, the potential degradation of health for lithium ion batteries can be presented by the change of impedance spectrum.

Some researchers also studied the lithium-ion battery by focusing on the slow aging process. Shogo Komagata et al. use acoustic method to detect Acoustic Emission (AE) which derived from bubble formation and particle fracture in charging/discharging cycling [40]. This method can detect either the gassing or particle falling off from which the materials on electrode gradually aging and defecting derived. Although it is an innovated method to study the battery in aging process, it is difficult to show the relationship between AE and battery failure quantitatively or qualitatively.

1.6 Lithium-ion Batteries Safety Test and Standards

With the rapid development of commercialization of lithium-ion batteries, the safety tests for lithium-ion batteries have been developed by numerous national or international organizations. All these tests are normally considered as representative of abnormal evens that can may occurs in mass-production or market. The safety tests for lithium-ion battery may sort in four groups which include the electrical tests, the mechanical tests, the thermal tests and the environmental tests. Each test group includes series of tests to test the batteries in assigned conditions or scenarios.

In electrical test group, the lithium-ion batteries are tested in overcharge, overdischarge, external short circuit, force discharge, pulse test etc.

In mechanical test group, the lithium-ion batteries are tested in drop, mechanical impact, nail piece, shock, crush, vibration, acceleration etc.

The thermal test group includes flame, sand bath, hot plate, thermal shock and so on.

The environmental test group includes operating temperature, decompression, altitude, immersion, fungus resistance and so on.

Up to date, many standards about lithium-ion battery safety test have been published by some related organization. Some existing lithium ion battery test standards are shown as follows:

• Underwriters Laboratories (UL)

o UL 1642 Standard for safety for Lithium batteries

o SU 2054 UL Standard for Safety Household and Commercial Batteries

• The Institute of Electrical and Electronic Engineers (IEEE)

o IEEE 1725 IEEE Standard for Rechargeable Batteries for Celluar Telephones

o IEEE1625 IEEE Standard for Rechargeable Batteries for Portable Computing

• International Electrotechnical Commission (IEC)

o IEC 61233 Secondary cells and batteries containing alkaline or other non-acid electrolytes - Safety requirements for portable sealed secondary cells and for batteries made from them, for use in portable applications

o IEC 62281. Ed.1. Safety of primary and secondary lithium cells and batteries during transport

o IEC 61960. Ed.1. Secondary cells and batteries containing alkaline or other non-acid electrolytes. Secondary lithium cells and batteries for portable applications

• United Nation (UN)

o UN 38.3 Lithium metal and lithium ion batteries

Besides, some countries also made standards for lithium-ion batteries safety test, such as,

• British standard

o BS 2G 239:1992 Specification for primary active lithium batteries for use in aircraft

o BS EN 60086-4:2000, IEC 60086-4:2000 Primary batteries. Safety standard for

lithium batteries

o BS EN 61960-1:2001, IEC 61960-1:2000 Secondary lithium cells and batteries for portable applications. Secondary lithium cells

o BS EN 61960-2:2002, IEC 61960-2:2001 Secondary lithium cells and batteries for portable applications. Secondary lithium batteries

• Chinese National standards

o GB /T18287-2000 Chinese National Standard for Lithium Ion batteries for mobile phones

• Japanese Standards Association and Battery Association of Japan

o JIS C 8712:2006 Safety requirements for portable sealed secondary cells, and batteries made from them, for use in portable applications.

1.7 Major Contributions of This Thesis Work

The contribution of this thesis work consists of three parts: simplifying thermal model of lithium ion battery, designing TDIS failure detector and selecting TDIS as a key parameter in lithium ion battery failure detection.

The model simplification is a key process in designing practical and efficient failure detector. The simplified model much reduced the calculation to make the real-time failure detector possible. In this thesis, a lumped simplified thermal model which includes the heat generation and propagation was built for a prismatic lithium ion battery. This model is simple and efficient to be used for TDIS detector in failure early detection.

The major different of the TDIS failure detector is that either heat generation error or heat propagation error can be detected in one detector. The TDIS detector only use charging/discharging current as input to detect battery failure by calculating aberrant heat generation and transportation in normal operating condition.

The TDIS is used as a key parameter to detect lithium ion battery failure is another major contribution of this thesis work. The temperature between internal point and surface is more stable and convenient in building model and measuring heating power in generation and propagation than the surface temperature. The early failure detector of lithium ion battery is come up with based on the introducing of TDIS parameter. The TDIS is validated by experiments as a convenient and appropriate parameter in heating power detection.

1.8 Organization of this Thesis

This thesis is oriented towards introducing and developing a practical method in lithium ion battery failure early detection based on the thermal characteristics of lithium ion batteries and a simplified model. In this regard, chapter 1 gives an overview and background knowledge for the necessity for battery modeling, detector design and introduces about temperature hazards, existing problems and state-of-the-art of failure detection. This is followed by a detailed explanation of the techniques in battery modeling in chapter 2. In chapter 3, the problem is defined and corresponding battery models is built by which the detectors based on TDIS is deducted. Chapter 4 presents the experiments which performed in validating the battery model and TDIS detectors. Chapter 5 discusses about the techniques in parameter estimation and analysis based on the experimental data. In chapter 6, the TDIS detector is designed, simulated and validated in summarizing the experimental data, built model and deducted equations. To conclude, chapter 7 summarizes the details of the TDIS detectors in advantages and drawbacks based on the results of validation. The conclusion is drawn and the possible scope of improvising on the implementation as a future is dealt with as well.

2. BACKGROUND WORK

2.1 Battery Failure Detection Strategies

According to Chapter 1, a lithium-ion battery is not safe enough. It can be hazarded or damaged in some unexpected conditions. To protect the battery, the unsafe conditions or errors must be found before the failure happens. In a battery module, a Protection Circuit Module (PCM) is responsible to detect the abnormal conditions which include over-voltage, over-current, overcharging or overdischarging, overheating and short circuit. The corresponding protection will act to protect battery from failure when these abnormal conditions are detected and over the preset severity level.

2.1.1 Introduction of Failures Detection in BMS

In a lithium-ion battery, the Battery Management System (BMS) is a system which manages batteries in a battery pack. The functions of BMS include cell protection, charge control, demand management, SOC determination, State of Health (SOH) determination, cell balancing, data log, authentication and identification, and communication. Normally, three management levels are applied in a battery pack. They are the pack level management, the module level management and the cell level management [41]. Among three levels, the cell management level pays more attention to failure detection and protection. Besides the power demand calculation, SOC determination, SOH determination, the major functions of the Battery Management System are to provide the necessary monitoring, detection to protect the cells from abnormal conditions which are out of tolerance ambient or operating conditions. To implement these protective functions, a PCM is attached to the battery module as

an independent unit of BMS to detect the signals and control batteries in normal operating state. Figure 2.1 shows a typical battery management system in a hybrid vehicle in which three management levels are all involved.

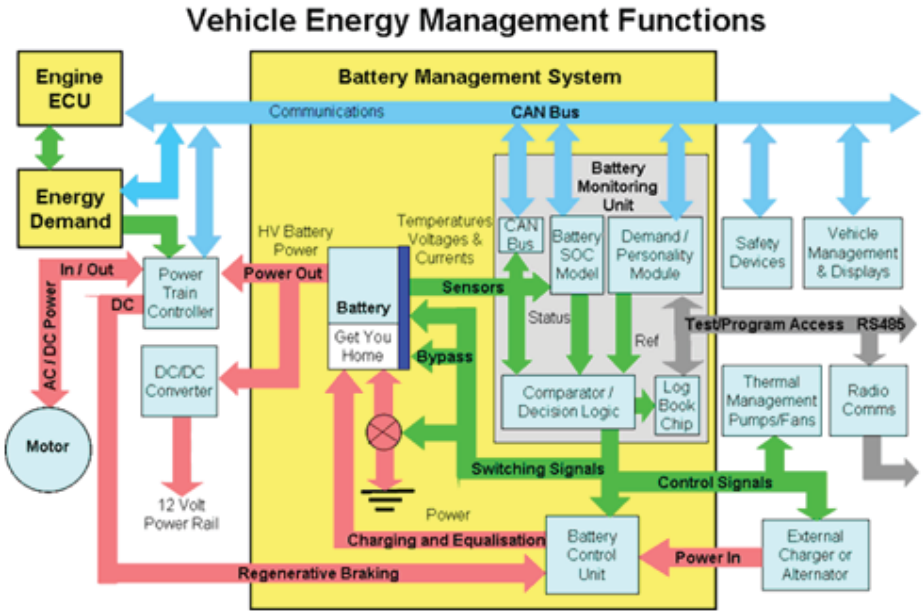

Fig. 2.1. An example of Battery Management System

As shown in Figure 2.1, the battery monitoring unit plays the role of PCM. The unit is responsible to gather real-time data such as voltage, current and temperature. And then the unit will calculate and judge the battery status. The corresponding action will be taken as soon as the faults are found and determined in different severities. For example, the batteries will be disconnected from the module or pack once short circuit occurs because the short circuit was defined in a high severity level. And, the cooling system starts to work if some batteries are detected to be overheating which is defined as relative lower severity level. The failure detection and protection is particular important in automotive applications due to the harsh working environment. The individual cell protection and failure detection for automotive system must be designed because all batteries in a pack are connected. The failure of individual cell is possible to exacerbate rapidly to result in catastrophic aftermaths.

2.1.2 Over-Charging Detection

Because of the electrochemistry of lithium-ion battery, the over-charge of lithium-ion battery may cause irreversible capacity loss and risk of burn and explosion. The overcharged cathode may bring on solvent oxidation and exothermic decomposition of active materials which results in changing chemical structure of cathode over time [41]. Therefore, the BMS system should be able to detect the over-charging condition to prevent battery being charged in this condition. The detection of over-charging is based on the SOC determination. Normally, the over-charging detection use voltage measurement method. If the battery voltage is over the upper limit, the BMS will think the battery in over-charging condition. The upper limit of voltage is normally set in a range of 3.65 V to 4.2 V. It depends on the type of lithium-ion batteries. For example, the upper limit for $LiCoO_2$ is 4.2 V. For a $LiFePO_4$ battery the upper limit can be as low as 3.65 V.

2.1.3 Under Voltage Detection

The under voltage, namely over-discharging can also cause capacity loss even permanent damage of lithium-ion batteries. The frequent over-discharging can impacts the life of battery negatively. Moreover, the low voltage can also damage electronic devices which use the batteries as power supply. So, the BMS system normally lock out the battery power to protect the battery from over-discharged and to prevent the electronics out of work in low voltage condition. The over-discharging also based on SOC estimation. Because SOC estimation varies with the ambient temperature, discharge current rate and the voltage of battery falls sharply when the battery discharged close to 0% SOC, the inaccurate SOC is dangerous to response over-discharge condition. To solve this problem, a fixed lower voltage limit is used to protect the battery from over-discharging. Because the voltage detection responses much faster than SOC estimation, the protection can act at more accurate time when the sudden

falling of battery voltage happening. For most of lithium-ion batteries, the lower voltage limit is set in 2.75 V to 3.0 V.

2.1.4 Short Circuit Detection

Short circuit is a serious failure to result in catastrophic aftermath in either single cell or Lithium ion battery pack because large amount of heat is generated to damage the batteries in high temperature. The short circuit occurs in two conditions - external short circuit and internal short circuit. The external short circuit happens at the outlet terminals and electrode. The short circuit can drop the output voltage close to zero. So, the short circuit at external position is easy to be found by voltage detection. Another type of short circuit is internal short circuit which happens in the internal position of a lithium ion battery. The internal short circuit may result from contacted internal electrodes, lithium plating in low temperature or large current, Copper or Aluminum Bridge by their ions transportation, broken separator, over charging and so on. The internal short circuit is more difficult to detect than external short circuit because the internal short circuit does not happen as harshly as external shot circuit. Moreover, the internal short circuit might occur intermittently sometimes. The hazard of internal short circuit is much more than external short circuit. The first, the internal short circuit damages the structure of battery directly. The second, the generated heat by internal short circuit is easier to accumulate in battery to result in high temperature even thermal runaway than external short circuit. The lithium ion batteries will be killed by internal short circuit directly in most case. Therefore, a good battery management system should have ability to detect internal short circuit. Normally, the internal short circuit can be detected by detecting voltage drop or abnormal temperature rising rate. In this thesis, a temperature detecting method will be developed to detect possible internal short circuit.

2.1.5 Over-Temperature Detection

For lithium-ion batteries, the thermal issue is very important aspect in safety design. Most of failures in lithium-ion battery are caused by excessive temperature directly or indirectly. To ensure the safety of lithium-ion battery, the operating temperature should be lower than 45°C in charging or less than 60°C in discharging. If the lithium-ion batteries are operated in higher temperature, it may result in accelerated aging or battery failure, or even a thermal runaway which can cause serious bad results such as fire or explosion.

In normal condition, the heat generated by a lithium-ion battery can be thought as two heating sources: the electrical resistive loss and chemical heat. For electrical resistive loss, the heat is always released when current flowing over the battery. However, the heat from chemical reaction is much different. In the process of charging, the electrochemistry reaction is endothermic which absorbs heat. In the process of charging, the electrochemistry is exothermic which releases heat [42]. The complexity of heating process makes the heat related study of lithium-ion batteries have to be divided in charging and discharging process respectively.

In laboratory, the heating power can be measured by instruments, such as Accelerating Rate Calorimeter (ARC), Isothermal Battery Calorimeter (IBC), or Differential Scanning Calorimeter (DSC). For example, Gnanaraj use ARC to measure heating power from the thermal reactions of Lithium-ion battery electrolyte solutions [43]. The instrument can obtain the precise heating power in specific test profiles. However, the high cost, niggling operation and complexity of implementation limits the application of calorimeters in BMS or over-temperature detection.

In practical application in BMS system, the popular method to protect lithium-ion batteries from over-temperature condition is to use some devices which have temperature detection and current-cutoff function. The devices include PTC, thermal fuse, reusable fuse and electronic circuit. A well-protected lithium-ion battery should have over-temperature build-in over-temperature protective device. The build-in sensors

or devices can cut off current when high temperature is detected to be over a fixed protective point. Thus, the lithium-ion batteries can be protected from the harm of high temperature. However, the method cannot monitor or predict the trends of temperature. The protective actions are only taken after high temperature happened. The batteries have already abused in the high temperature condition. The precaution or warning cannot be given in the early time of battery failure.

Another method is on-line temperature monitoring. The on-line temperature monitoring systems regularly work with a temperature control system to keep the temperature in normal operating range. To supervise temperature fluctuation which varies with the internal or ambient conditions, the control system needs an input reference of temperature which represents the normal operating temperature at measured point which can be predicted based on mathematical model in terms of certain input parameters such as current, voltage, ambient temperature or SOC. Because of the complexity of temperature expression, the practical method has not been found in literatures from which the battery temperature can be predicted precisely in lithium battery application until now. In spite of this, some approximation methods to predict battery temperature by dynamic model have been built. For example, In Zhijian James Wu's patent, the internal temperature can be predicted based on battery dynamic model. By this method, the temperature at certain point in a battery can be calculated when the battery is operated in normal condition. However, this method is too complex to implement in lithium-ion battery pack. A simple, low cost method for on-line temperature estimation is still needed in lithium-ion battery application.

2.2 SOC Estimation

The state of charge (SOC) is a measure of the amount of electrochemical energy left in a cell or battery. The SOC shows how much energy in the battery can be delivered to the user. The unit of SOC is percent points (0% = empty, 100% = full). The SOC is the opposite of the Depth of Discharge (DOD) in that 60% SOC =

40% DOD. In a battery, the SOC cannot be measured directly. Therefore, the SOC must be derived from other physical parameters. Normally, the SOC value can be estimated by following methods [44]:

- Direct measurement
- Book-keeping estimation
- Adaptive SOC estimation

Each method will be explained in detail as follows.

2.2.1 Direct Measurement

The direct measurement determines SOC by some physical parameters such as voltage (V), battery impedance (Z), temperature (T) and voltage relaxation time (τ) after application of a current step. The basic principle of direct measurement can be described by following function.

$$SOC = f(T, V, Z, \tau) \tag{2.1}$$

The SOC can be calculated in terms of the voltage relaxation time, voltage, impedance and temperature. In direct measurement method, the voltage measurement is the most popular method, especially, for mobile phone application. The voltage-based estimation method calculates SOC roughly by the relationship of battery voltage and SOC [45]. Figure 2.2 shows a typical discharge curve of a lithium-ion battery. The SOC can be read by the voltage on the curve. However, the voltage is not proportional to the SOC. The voltage sharply drops in both of the charge beginning and ending. So, it is not accurate in the two periods.

Another common method is the EMF method. EMF stands for electromotive force which can be inferred from thermodynamic data and Nernst equation to determine SOC [46]. Three of practical EMF method are often used in SOC estimation.

- Look-up table

In look-up table method, the fixed values of measured EMF parameters can be stored.

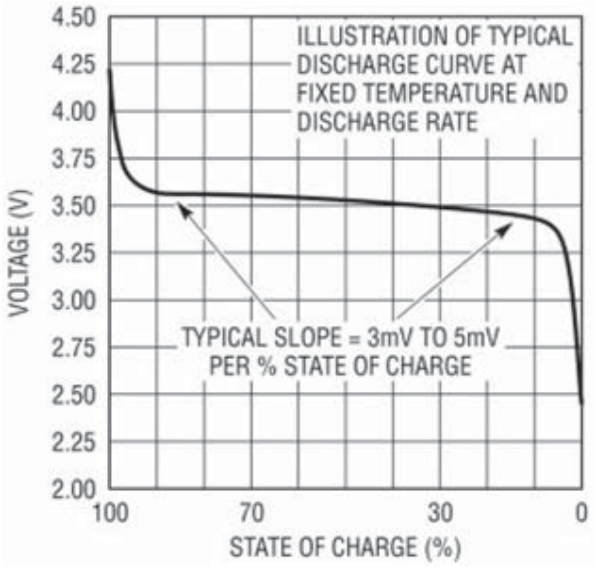

Fig. 2.2. Typical discharge curve for a lithium-ion battery

The SOC can be indicated by looking up these values.

• Piecewise linear function

In this method, the EMF curve is fitted with Piecewise linear function. The SOC can be calculated by each Piecewise section.

• Mathematical function

The SOC value also can be calculated with a mathematical function. For example, the SOC can be approximated from the EMF value which derived from the model of difference equilibrium potentials of positive and negative electrodes [46].

The impedance measurement can also be used in direct measure method. The internal impedance of a lithium-ion battery can be presented by complex impedance which stands for the ratio of complex voltage and complex current. The internal impedance normally is measured by Electrochemical Impedance Spectroscopy (EIS) method which can measure internal impedance by frequency scanning of AC voltage [47]. The SOC can be estimated once the curve of internal impedance versus SOC was obtained. But, there is a drawback for this method. That is the measurement of

internal impedance is not practical in application of lithium-ion battery due to the sophisticated test instrument.

2.2.2 Book-Keeping Estimation

The Book-keeping is a method for SOC indication that is based on both current measurement and integration [46]. The basic definition of SOC is the charge, namely the integration of current. This definition can be described by equation:

$$SOC = \int i(t)dt \tag{2.2}$$

Where, C is the capacity of the lithium-ion battery. Therefore, SOC can be understood as the accumulation of charged or discharged current over time. The Book-keeping method can calculate SOC more accurately than voltage-base methods. However, this method still has some drawbacks. The first, the SOC estimated by this method can be affected by operating temperature, self-charging rate, charging current and the aging factor. So, the SOC value needs to be corrected by these factors. The second, the SOC needs to be calibrated or reset periodically due to the accumulative errors. So, if the accurate SOC is required in applications, the calculation of SOC by Book-keeping method must be referring to the operating temperature, self-discharging, charging current rate, aging and other factors which can influence on the integration of current.

2.2.3 Adaptive SOC Estimation

The adaptive SOC estimation method was developed based on direct measurement method or Book-keeping method or combination of the two [46]. Normally, A SOC estimator is difficult to be accurate because the battery behavior and user behavior are both unpredictable. To solve this problem, some adaptive methods are introduced to estimate SOC. For example, the Kalman filters can be implemented in connection with parameter estimation to determine SOC. Plett gives a practical method to estimate

SOC by identifying the unknown parameters in a cell with extended Kalman filter (EKF). Moreover, the artificial neural networks(ANN) is also employed to model system parameters to adapt the prediction of current curve to the general behavior of the battery pack. Chenhui Cai designed a SOC estimator for high power Ni-MH battery with ANN algorithm. Besides, some other more effective algorithms also are used in the SOC estimation. For instance, Pen Jinchun and Yaobin Chen use a modified particle swarm optimization (PSO) algorithm to train the proposed neural network in SOC estimation with errors less than 5%.

2.3 State of Health (SOH) on Battery Thermal Characteristics

The state of health (SOH) is a Figure of Merit (FOM) of the condition of a battery which compare to ideal conditions. The unit of SOH is percent point. Typically, the SOH of a battery is 100% at the time of leaving factory. In the life of a battery, the SOH will be deceased over time until the battery is dead.

Because the SOH is a symbol to indicate the battery condition relative to a new battery, a diagnostic system should be made to hold the characteristics of a battery in initial condition. The system should be able to monitor the parameters and compare to initial state and analyze the SOH. In the meantime, a profile should be created to keep the state of the parameters in memory as the references for future diagnostics. The profile can also work with state of life which is derived from the charging/discharging cycle of a battery to indicate the SOH by aging effects because the life of a lithium-ion battery fairly depend on the state of health.

The definition of SOH maybe variable because it depends on what parameters can indicate the health of battery in different conditions. For example, the capacity loss can show the battery health in capacity reduction over time. Therefore, the capacity loss can be defined as a figure of SOH to indicate the loss of ability to store energy. Besides that, the OCV also can be used to indicate the SOH of batteries. The curve of OCV will change significantly with age. If the abnormal OCV is detected in certain

SOC point, it will signify that some internal changes have happened which may cause risk of failure of a lithium-ion battery. The battery is reducing in SOH. Because the variety of definition of SOH, it is difficult to make a uniformed standard of SOH up to date.

The temperature is also an important parameter to indicate the SOH of a lithium-ion battery. Many potential factors which cause failure of a battery relate to the thermal performance of the battery. If the temperature of battery increases sharply in normal operating condition, it indicate that some internal wrongs probably happened such as internal short circuits, broken separator, unpredicted chemical reaction. This battery should be defined in bad health in this condition. In practice, only few systems use temperature for SOH estimation especially the failure detection due to the slow response and complexity of involved factors. Many factors can work on the thermal behavior of a lithium-ion battery, therefore, the expression of temperature change would be a very complex equation which involves hundreds input parameters in electrochemistry, fluid dynamic, thermal dynamic, geometry and electrical characteristics. Therefore, it is very difficult to make a accurate thermal model for on-line monitoring in practice. The complexity of the SOH diagnostic system requires a embedded microprocessor to deal with the massive data and parameters, in practical application, the capability of calculation for a microprocessor is fairly limited. So, the practical algorithms and models for SOH estimation must be simplified to match the capability of a microprocessor in BMS system.

3. THERMAL MODEL OF LITHIUM-ION BATTERIES

As discussed in chapter 2, most of catastrophic failures of lithium-ion batteries are initiated by rapid increasing temperature. If the abnormal thermal behavior can be caught in early time of battery failure, the battery will be saved from extreme dangerous risks such as burning and explosion. To study the thermal behavior, a thermal model is required to estimate the parameters in heat generation and thermal dynamic in a lithium ion battery. A relative stable parameter for rating the battery status is also required because the values in thermal model are changed under various conditions of SOC, temperature, and charging/discharging rate due to the physical phenomena in the lithium ion batteries. Under this study, the temperature difference between internal point and surface (TDBIS) is used as a key parameter to estimate the state of health in thermal behavior in a lithium-ion battery. The thermal model for TDBIS will be developed in this chapter as follows.

3.1 Heat Generation in a Lithium-ion Battery

3.1.1 The Factors to Generate Heat in a Lithium-ion Battery

In a lithium-ion battery, the heat is generated from three sources: the electrical resistive heat, chemical heat and physical heat. According to the equation of Thomas and Newman, the heat generated or consumed can be expressed as follows [48].

$$\dot{Q} = I(V - U^{AVG}) + IT\frac{\partial U^{AVG}}{\partial T} - \sum\nolimits_i \nabla H_i^{AVG} r_i - \int \sum\nolimits_j (\overline{H}_j - \overline{H}_j^{AVG})\frac{\partial c_j}{\partial t} dv \quad (3.1)$$

Where, $\dot{Q}$ is the rate of heat generated or consumed

V is the cell voltage

U is the equilibrium potential

I is the current

T is the temperature

H_i is the variation of enthalpy of a chemical reaction i

r_i is the rate of reaction i

$\overline{H}_j$ is the partial molar enthalpy of species j

c_j is concentration

t is the time

v is the volume

The "AVG" of superscript indicate the parameters are developed at the volume-averaged concentration. In this equation, the four items represent different aspects in electrical, chemical and physical processes respectively. The first item shows the electrical heat generated by internal resistive impedance. The second shows the heat generated by reversible entropic heat. This item can be either positive or negative. The third item stands for the reversible entropic heat by any chemical reactions in a lithium-ion cell. It is either positive or negative as well. In the lithium-ion cell under consideration in this study, side reactions accounting for aging are pretty slow to be ignored. So is the third item in equation 3.1 as well. The forth item represents the mixing heat in a cell from which is resulted the process of formation and the change of concentration. This item can be either big or small depending on the design of the structure of the cell. Under the consideration in this study, this item can also be neglected because the batteries for this test are designed for large current application. The gradient across porous electrodes and separators is too small to be ignored. The mixing heating can be either positive or negative. In the four items, electrical and chemical heat takes overwhelming majority [48]. The physical heat associated to the electrochemical reaction in a lithium-ion battery can be ignored due to the trivial amount. Therefore, the equation can be simplified to leave only electrical and chemical heat parts.

The electrical heat is also called Joule Heat. The electrical heat was generated by the resistive losses as current flows through the internal resistance in the lithium-

ion battery. The electrical heat is always positive in either charging or discharging process.

The reversible entropy is another important part of heat source in a lithium-ion battery [49]. The reversible entropy can be either positive or negative that depend on the type of electrochemical reaction and the state of intercalation of the crystal layers in a lithium-ion battery. The endothermic reactions take place initially and then moving to exothermic gradually in the battery during the charging process. In the discharging process, the process goes the reverse. So, the majority of entropic heat is positive in discharging process.

Base on the characteristics of heat sources in a lithium ion cell, the majority of heating power comes from electrical heat and reversible entropy. Therefore, in this study, the electrical heat and reversible entropy are only considered. The heating power of lithium ion batteries can be simplified as equation (3.2)

$$\dot{Q} = I(V - U^{AVG}) + IT\frac{\partial U^{AVG}}{\partial T} \tag{3.2}$$

The heating power can also be expressed as resistive loss as equation (3.3).

$$\dot{Q} = I^2R + IT\frac{\partial U^{AVG}}{\partial T} \tag{3.3}$$

Where, R is the total internal resistance in a lithium ion cell. According to equation 3.3, the major factors to generate heat in lithium ion batteries are all related to the input current. For this reason, the input current is applicable to be a input parameter for describing the heat generation in a thermal model.

From above equations, it can be seen that it is difficult to calculate accurate heating power due to the unclear mechanism of heat generation. Moreover, the equations are too complex to implement in real-world applications. Therefore, in this thesis, the direct measurement is used to obtain the standard heating power reference instead of direct calculation. The models for the measurement will be built and validated in next chapters.

3.2 Thermal Model of a Lithium-ion Battery

3.2.1 Heat Transfer in a Lithium ion Battery

As the thermal model for a lithium-ion battery by Kumareasan,the physical principles govern the behavior of the thermal dynamic in lithium-ion batteries [50]. As has been noted in last section, the heat generated or absorbed by a lithium-ion a battery is supposed to be balanced according to the law of energy conservation. The heating energy balance can be represented in a lithium ion battery in the following equation.

$$C_p \frac{\partial T_i}{\partial t} + q_i = \dot{Q} \tag{3.4}$$

where, C_p is the heat capacity, T_i is the internal temperature of the cell, t is the time, q_i is total heat transferred to the air, $\dot{Q}$ is the total heating power which is generated or absorbed by a lithium ion cell. The heat flux across the internal point and surface should be same as the heat flux across the surface to the air if we assume that no heat energy is converted to other forms of energy. Therefore, q_i can be represented as.

$$q_i = \frac{\Delta T_{TDIS}}{R_{th\_c}} \quad or \quad q_i = \frac{\Delta T_{TD\mathrm{SA}}}{R_{th\_a}} \tag{3.5}$$

where, ΔT_{TDIS} is the temperature difference between internal point and surface, R_{th_c} is the thermal resistance between the two points, $\Delta T_{TD\mathrm{SA}}$ is the temperature difference between surface and air, R_{th_a}) is the thermal resistance between surface and air. The equation can also be written as,

$$C_p \frac{\partial T_i}{\partial t} + \frac{\Delta T_{TDIS}}{R_{th\_c}} = \dot{Q} \tag{3.6}$$

or

$$C_p \frac{\partial T_i}{\partial t} + \frac{\Delta T_{TD\mathrm{SA}}}{R_{th\_a}} = \dot{Q} \tag{3.7}$$

Equation (3.6) describes the total heating power by the sum of internal temperature derivative and the temperature difference between internal point and surface. Equation (3.7) represents the total heating power by the sum of internal temperature derivative and the temperature difference between surface and air. Therefore, either equation (3.6) or equation (3.7) can be used to build a thermal model for estimating the heating power in a lithium ion battery if the temperature sensors are set in different position in or on the battery. According to equation (3.6), the temperature sensors should be set at an internal point in the battery and a surface point on the lithium battery. The thermal behavior in the lithium ion cell can be modeled and simulated in this condition. On the other hand, Equation (3.7) describes the thermal behavior at the interface of battery package and air. A non-destructive method can be developed by modeling the thermal behavior on the surface and air according to Equation (3.7). The sensing points of temperature should be set at the surface of the battery and a point at which the surrounding temperature can be measured. In this study, Equation (3.6) will be used to study the thermal behavior which occurs inside the lithium ion batteries.

The heat that is transferred in a lithium ion battery is much different from that between surface and air. In the lithium battery, the majority of heat transportation is conduction. On the surface of battery, the heat is exchanged to the air by convection and radiation. Because the process of convection and radiation is governed by lot of physical parameters such as temperature, air pressure, moisture, state of the surface and position of surrounding objects, the thermal resistance between surface and air is too complex to analyze and simulate accurately [51]. Therefore, the heat transferred in solid is more stable than that on the interface of solid and air. The temperature difference between internal point and surface (TDIS) is more suitable as a key parameter to build thermal model and to describe the thermal behavior in lithium ion batteries.

3.2.2 Lumped Model for a Prismatic Lithium ion Battery

In this thesis, a prismatic was chosen for TDIS experiments. The battery has shape of cuboids. Just as shown in Figure 3.1, the battery has 6 faces and fixed volume. We assume the center of the heat distribution in the center of the battery. The heat is generate and transferred from center to each faces and dissipate to the surrounding air. If the total heating power is Q, the heating flux power in the direction of forward, backward, upward, downward, leftward and rightward are respectively Qf, Qb, Qu, Qd, Ql and Qr. The total heating power should equal the total heat which is transferred to surface.

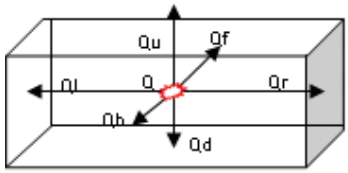

Fig. 3.1. Heat flux transfer in a prismatic lithium-ion battery

$$Q = Q_f + Q_b + Q_u + Q_d + Q_l + Q_r + C_p \frac{\partial T_i}{\partial t} \tag{3.8}$$

This equation can also be represented as,

$$Q = \frac{\Delta Tf}{Rth_f} + \frac{\Delta Tb}{Rth_b} + \frac{\Delta Tu}{Rth_u} + \frac{\Delta Td}{Rth_d} + \frac{\Delta Tl}{Rth_l} + \frac{\Delta Tr}{Rth_r} + C_p \frac{\partial T_i}{\partial t} \tag{3.9}$$

where,

ΔTf is the TDIS in forward direction

ΔTb is the TDIS in back direction

ΔTu is the TDIS in upward direction

ΔTd is the TDIS in downward direction

ΔTl is the TDIS in leftward direction

ΔTr is the TDIS in rightward direction

Rth_f is the thermal resistance between internal point and surface in forward direction

Rth_b is the thermal resistance between internal point and surface in backward direction

Rth_u is the thermal resistance between internal point and surface in upward direction

Rth_d is the thermal resistance between internal point and surface in downward direction

Rth_l is the thermal resistance between internal point and surface in leftward direction

Rth_r is the thermal resistance between internal point and surface in rightward direction

C_p is the thermal capacitance of the battery

The heat transfer on the surface is different from that in battery. On the surface of a lithium ion battery, the convection and radiation effect on the heat transportation explicitly. Therefore, to describe the process of heat dissipation clearly, the thermal resistance is classified to convective thermal resistance and radiative thermal resistance respectively. The thermal resistance between surface and air can be described as the connection of a convective thermal resistor and a radiative thermal resistor in parallel. Thus, the heat flux on battery surface can be represented as following equation.

$$Q = \Delta T_{a_f}/(Rth_{con_f}||Rth_{rad_f}) + \Delta T_{a_b}/(Rth_{con_b}||Rth_{rad_b}) + \Delta T_{a_u}/(Rth_{con_u}||Rth_{rad_u}) + \Delta T_{a_d}/(Rth_{con_d}||Rth_{rad_d}) + \Delta T_{a_l}/(Rth_{con_l}||Rth_{rad_l}) + \Delta T_{a_r}/(Rth_{con_r}||Rth_{rad_r}) \tag{3.10}$$

where, Q is the total heating power of a lithium ion battery

ΔTa_f is temperature difference between surface and air in forward direction

ΔTa_b is temperature difference between surface and air in backward direction

ΔTa_u is temperature difference between surface and air in upward direction

ΔTa_d is temperature difference between surface and air in downward direction

ΔTa_l is temperature difference between surface and air in leftward direction

ΔTa_r is temperature difference between surface and air in rightward direction

Rth_{con_f} is the convective thermal resistance in forward direction

Rth_{con_b} is the convective thermal resistance in backward direction

Rth_{con_u} is the convective thermal resistance in upward direction

Rth_{con_d} is the convective thermal resistance in downward direction

Rth_{con_l} is the convective thermal resistance in leftward direction

Rth_{con_r} is the convective thermal resistance in rightward direction

C_p is the thermal capacitance of the battery

Regarding the temperature distribution in each face of a lithium ion battery, a detailed lumped model can be built by combining the conditions for the heat flux transferring from center of the battery to surrounding air. This model follows the heat flux which starts at a temperature point in the center of the lithium battery and end at a temperature point of air. Figure 3.2 shows the detailed lumped model for a lithium-ion battery.

The detailed lumped model is too complex to use. Too many parameters need to be determined in this model. To validate this model, a lot of temperature sensors and data acquisition devices are required in experiments. The complexity of the circuit also limits the applications in practice. Therefore, a simplified model is proposed to make the temperature measurement and analysis easier.

$$Q = \frac{TDIS}{Rth_{tdis}} + C_p \frac{\partial T_i}{\partial t} \tag{3.11}$$

If we assume that the thermal media inside the lithium batteries is approximate solid, the heat propagation should be uniform in lithium battery due to the symmetry shape. The internal thermal resistors can be merged in one signal thermal resistor. The simplified model inside battery can be represented in Equitation 3.11. This thermal resistor should be relative stable in thermal resistance in battery normal operating temperature in solid thermal media. Also, the thermal resistor on surface and in air can be combined in a standalone thermal resistor. The simplified model outside battery can be represented in Equitation 3.12 below.

$$Q = \frac{\Delta Ta}{Rth_a} + C_p \frac{\partial T_i}{\partial t} \tag{3.12}$$

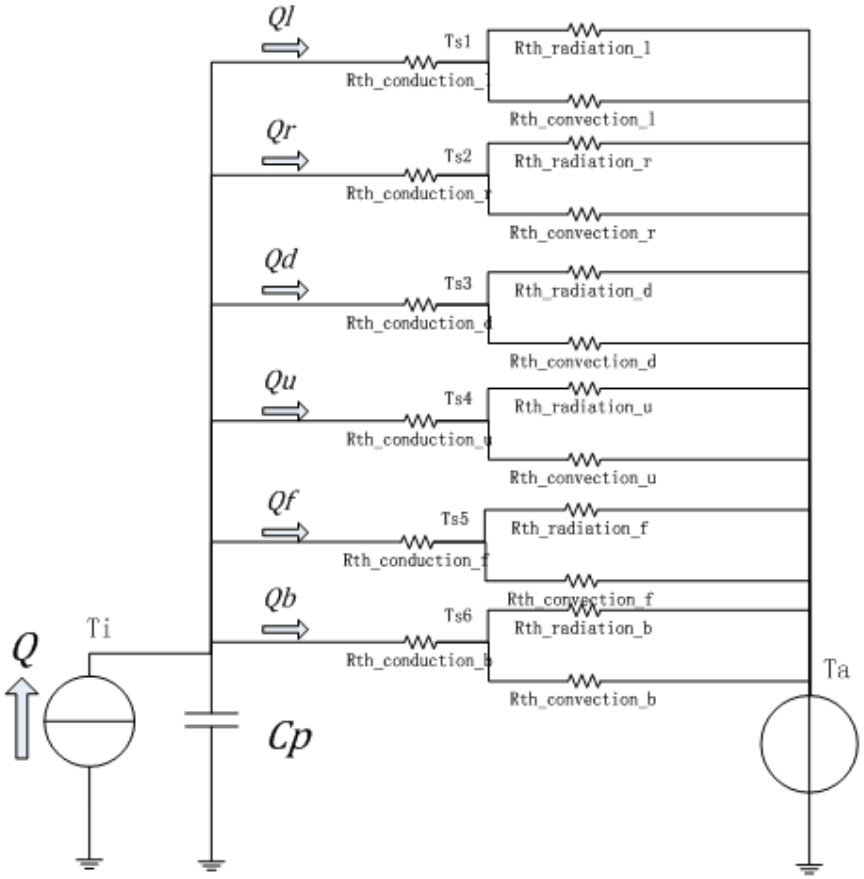

Fig. 3.2. Detailed Lumped model for a lithium-ion battery

In Figure 3.2, the simplified model is built to describe the temperature transportation from internal point to surrounding air. The equivalent thermal circuit is shown in Figure 3.3. The simplified model has only three components. The C_p represents the thermal capacitor in the lithium ion battery. The Rth_tdis stands for the thermal resistor between an internal point and surface. The Rth_a stands for the thermal resistor between surface and air. Ti, Ts and Ta stand for internal temperature, surface temperature and ambient temperature respectively. The three quantities are all measurable in test by setting temperature sensors in an internal point, a surface point and an ambient point respectively. The simplified model is more suitable for practical test and analysis because only three parameters need to be determined by

experiments. The TDIS of the battery can be obtained from simple measurements easily.

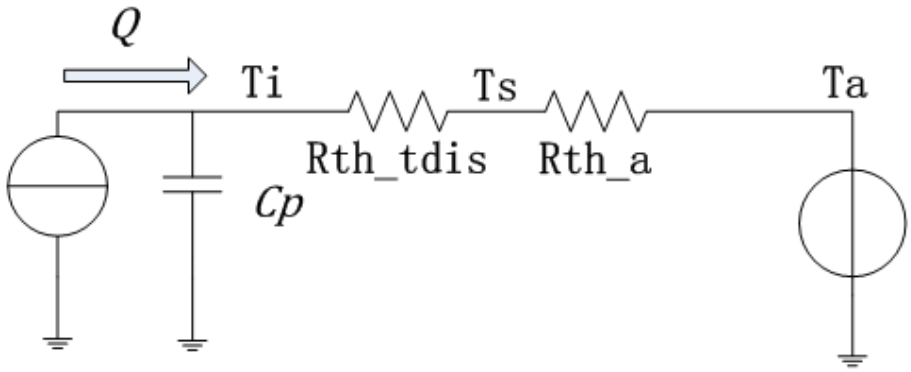

Fig. 3.3. Simplified lumped model for a lithium-ion battery

3.3 System Transfer Function for Simplified Thermal Model

Like the body temperature of mammals, the lithium ion battery also has temperature curve under certain conditions. If the temperature can be predicted as function of inputs such as current, voltage or ambient temperature by system dynamic, the temperature response to system input quantities can be used as reference to judge thermal failure. It means that the measured temperature will derivate the normal reference curve if an extra heating power intrudes the normal thermal system of the lithium ion battery. Some potential failures would be hinted by this intruded power because the extra power presents some failures such as aged components, loss contract or slight internal short circuit.

In this thesis, the TDIS is used to estimate heat generation of cell instead of the surface temperature used in traditional methods. In traditional methods, the temperature of surface is usually used for battery health state detection. However, a vital shortcoming of this method is the surface temperature is easily conditioned by ambient environments. The variations of surface temperature are resulted largely

from the variable ambient parameters. This makes the surface temperature difficult to estimate and calculation. In the proposed method, the potential failures are detected using temperature difference between surface and internal point (TDIS). Because the internal solid construction of cells is more stable than surface, the temperature difference between surface and internal point on the way of heating power flux is fixed in constant heating power. Thus, we can obtain a relative stable temperature reference to estimate the heating power in lithium ion batteries. Therefore, the model for system responses with TDIS will be developed to estimate input power in a lithium ion battery as follows.

Just as shown in the simplified model in Figure 3.3, the heat generated in a lithium ion battery will be transferred in two ways. Some heat accumulates in the battery to heat or cool battery in changing battery temperature. The C_p in the model can realize the function of heat accumulation. Other heat will be carried to the air by conduction and dissipation to create temperature gradient in the thermal resistors on the way of heat flux. The Rth_tdis is the thermal resistor which results in TDIS. The Rth_a is the thermal resistor which creates the temperature difference between surface and surrounding air.

The accumulation of heat in the lithium ion battery causes the temperature rise. According to the simplified model, the rate of temperature rise can be represented as $\frac{dT}{dt}$. The rate of heat accumulation can be given as,

$$Q_C = C_p \frac{dT}{dt} \tag{3.13}$$

Where Q_C is the rate of heat accumulation to the body of lithium ion battery, C_p is the heat capacity of the air occupying the body of the lithium ion battery.

The heat transfer rate by conduction in the body can be represented as,

$$Q_d = -\frac{(Ti - Ts)}{R_{th\_tdis}} = -\frac{TDIS}{R_{th\_tdis}} \tag{3.14}$$

The $-R_{th\_tdis}$ is a proportional constant called thermal resistance which is relative stable in solid thermal media. So, the total heat power can be represented as Equation (3.15) below,

$$C_p \frac{\partial T_i}{\partial t} + (\frac{\Delta T}{R_{th\_tdis}}) = \dot{Q} \tag{3.15}$$

Taking Laplace transformation on above equation will yield,

$$\Delta T(s) = \frac{\frac{1}{R_{th\_tdis}}}{R_{th\_tdis} * C_p * s + 1} Q(s) \tag{3.16}$$

The TDIS can be solved if the R_{th_tdis} and C_p are given. Where, R_{th_tdis} is the thermal resistance between internal and surface C_p is the thermal resistance of the battery $\Delta T(s)$ is the output temperature difference between internal and surface $Q(s)$ is the input heating power Assuming $\tau = R_{th\_tdis} * C_p$, the equation 3.17 can be wrote as,

$$\Delta T(s) = \frac{\frac{1}{R_{th\_tdis}}}{\tau s + 1} Q(s) \tag{3.17}$$

Thus, the relation of TDIS and input heating power is described as a first order system. The transfer function is,

$$\frac{\frac{1}{R_{th\_tdis}}}{\tau s + 1} \tag{3.18}$$

Because the transfer function is obtained, the system dynamics can be described as TDIS output which responds to system inputs. Moreover, the propagation delay should be also considered to improve this model. The measured temperature signal is delayed due to the lagging of heat transportation. If the time constant of delay is τ_d, the factor for delayed signal can be written as $e^{-\tau_d s}$. The improved equation with propagation delay is shown as follows.

$$DeltaT(s) = \frac{\frac{1}{Rth\_tdis}}{\tau s + 1} e^{-\tau_d s} Q(s) \tag{3.19}$$

In this model, only three parameters Rth_{tdis}, τ and τ_d need to be determinate by experiments. The thermal dynamic behavior can be predicted by this transfer function if the input power is known. The above equations can also be illustrated as in Figure 3.4,

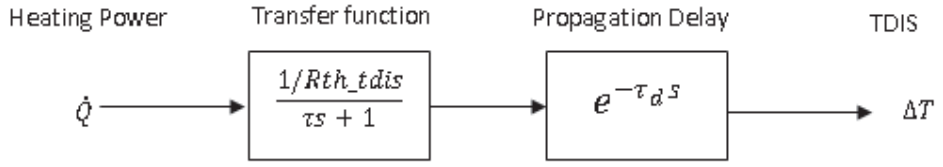

Fig. 3.4. Block diagram for thermal dynamic process in a lithium-ion battery

In summary, the TDIS can be used as a key parameter to provide information about the heating rate of lithium batteries if the transfer function of thermal dynamics is known. The input power can be used as a reference to estimate the dynamic temperature change which responds to input heating power by the transfer function. In other words, the temperature difference between internal point and surface can be monitored in real time if the heating power of lithium batteries in normal operating condition is obtained as a function of current, voltage, SOC or ambient temperature.

4. EXPERIMENTAL TESTS

Experimental tests were conducted on the lithium ion batteries in order to obtain the experimental results for model identification, parameter estimation and detector validation. Three kinds of experiments were performed on the batteries. The experiments include propagation delay test, cyclic constant current charge/discharge test and thermal runaway test.

4.1 Propagation Delay Test

In the measurement of TDIS, the measured signal should be delayed behind the input signal due to the heat flux transportation. If it is supposed that the heat source is located in an internal point of the battery and the sensors are physically located at a certain distance from the heat source and measuring point. The delayed signal makes the measured signal lagged in following real signal when the heat flows over the two points over a period of time. Therefore, the delay time should be known to make the measured signal synchronize to the output signal of thermal model. The propagation delay will be measured in this experiment.

4.1.1 Battery Modification

In this experiment, the lithium ion battery should be modified to fit the requirement of the test. A commercial lithium-ion battery from UNIONFORTUNE was selected for the TDIS measurement. This battery has a jellyroll structure, polymer package and flat shape. To measure the TDIS, two temperature sensors were placed in the center and the surface of battery, respectively. However, it is not easy to place sensors in the lithium ion batteries. First, the battery must be isolated to the air. Sec-

Table 4.1
The specifications for the lithium-ion battery in this test

Battery Code	E603048
Manufacturer	Unionfortune
Structure	Wound electrode
Type	Polymer lithium-ion battery
Capacity	900 mAh
Maximum Current	6A
Voltage	3.7V
Impedance	less than 300m
Working temperature	0 to 60 C
Dimensions	0.23x1.16x2.0" (5.84x29.5x51mm)
Weight	Appro.15g

ondly, the cell must keep tight laminated structure to have maximal contact surface in each layer. To overcome those problems, the battery should be modified with easy seal and minimal damage in structure. Therefore, the jellyroll type battery and foil type thermocouple couple were chosen for TDIS experimental test. The specification of the selected battery and thermocouple is shown in below tables.

The specifications of the lithium ion battery and size are shown in Table 4.1 and Figure 4.1.

The specifications of the thermocouple are shown in Table 4.2

According to the specifications of lithium ion battery and thermocouple, the thermocouple fit the requirement for modifying the battery in TDIS measurement. The thickness of the thermocouple is only 0.0005 in which the thermocouple can be inserted to the space in the center layers. The polyamide pad of the thermocouple can prevent the thermocouple from rolling, moving and chemical eroding in the battery as well. The structure of the cell is shown in Figure 4.2.

Table 4.2
The specifications of thermocouples for this test

Part	20112L
Manufacturer	Rdf Corporation
Thermocouple type	Chromel/Alumel Type K
Foil thickness	0.0005
Lead Dimension	30 DWG
Temperature range	-320 to 500F
Dimensions	0.0005x0.37x0.75”

Fig. 4.1. The shape and size of the lithium-ion battery width, length and height

The modification in the battery includes disabling protection circuit and inserting the thermocouple in the center position of the battery. The protection circuit can protect the lithium ion battery from overcharge, over-discharge, over current. The circuit can also have function in charge detection after overcharge and power down after over-discharge. However, the protection function will affect the experiments in overcharge, over-discharge, internal impedance test and thermal runaway test. So, the protection function of the protection circuit should be turned off in the modification.

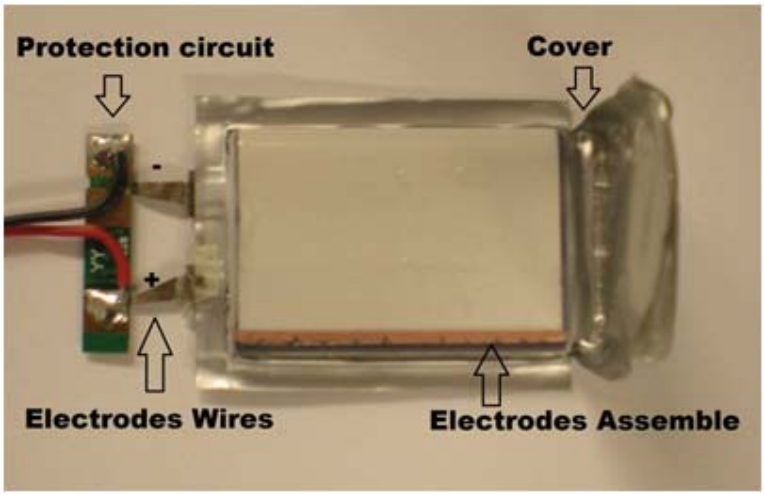

Fig. 4.2. The structure of battery before modification

The modified battery is shown in Figure 4.3. The protection circuit has been disabled by shorting the negative wire to negative outlet wire of the cell. And, the thermocouple is inserted in the same layer as the wire outlet. The measuring point is close to center point of the battery as marked as red dot in Figure 4.3.

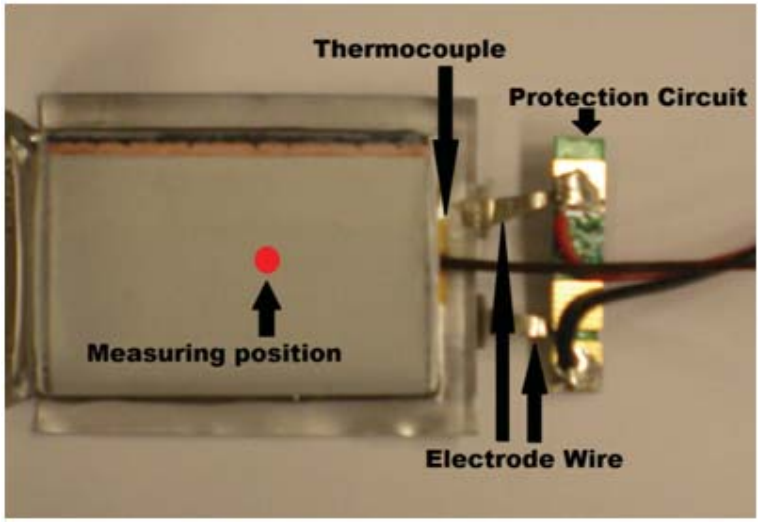

Fig. 4.3. The modified battery with thermocouple in the center position

The modified battery is sealed by silicon glue in order to isolate the battery to moisture due to the sensitivity of water in lithium battery. The modified battery can still maintain the charging and discharge characteristics in a short period because the built-in thermocouple does not hurt the structure of battery. It assures that the modified battery has similar performance as unmodified battery. And, the test results should be comparable and close between modified and unmodified batteries. The battery modification is operated in low moisture glove box to reduce the reaction between electrolyte and water vapor in air as much as possible.

4.1.2 Experimental Set-up

The circuit diagram of experimental setup is shown in Figure 4.4. The circuit consists of an electrical measurement circuit and a temperature measurement circuit. In the electrical measurement circuit, the voltage and current of the modified lithium ion battery is measured by Solartron 1470E Cell Tester. The 1470E can discharge or charge the lithium ion battery and record the value of current and voltage on the terminal of the lithium ion battery by setting experiments and measurements in Multistat software on a control computer. The temperature at internal point, top surface point and bottom surface point is measured by thermocouples. The thermocouples are also connected to Solartron cell tester via an adapter as shown in the figure. In this test, three channels were used to measure the temperature. The Solartron cell tester can also record the value of temperatures and work with the current and voltage sampling synchronously.

The photo for the experimental setup is shown in Figure 4.5. The modified battery and thermocouples are assembled as a test sample which is placed in a thermostatic safety chamber. The safety chamber can protect the testing battery from the risk of explosion, burn and electrolyte leakage. This camber can also adjust ambient temperature by a thermostat to keep the surrounding temperature remaining constant in the test. In the test setup, all the cables are shielded to immune the electrical noise.

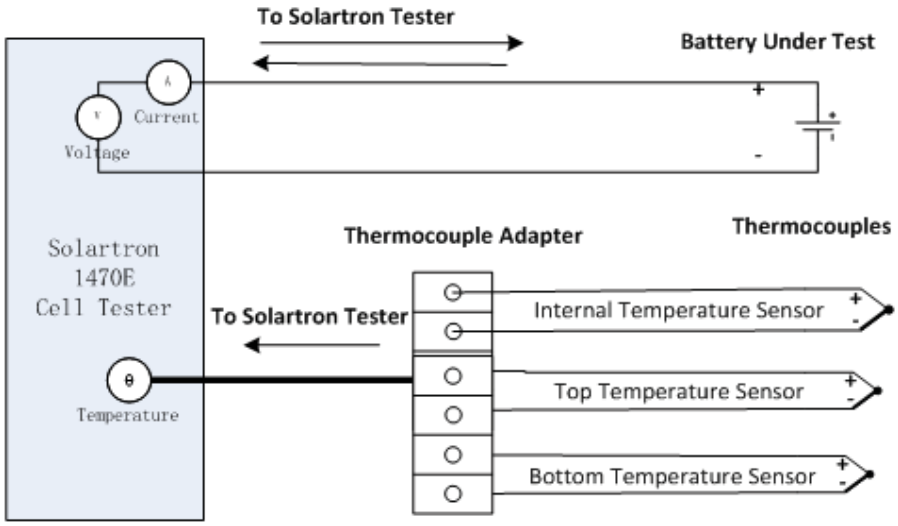

Fig. 4.4. The experimental setup

4.1.3 Propagation Delay Test

The measured temperature follows the input current signal with a propagation delay time due to the heat propagation in measuring points. In this test, three temperature sensors are placed in top surface, center and bottom surface. The test circuit is setup as shown in Figure 4.1.4. In this test, a pulsing method is employed to obtain the delay time between input current signal and temperature change which respond to the input signal. The battery is heated up by input current pulse. The temperature at the points of internal, top surface and bottom surface will rise up and drop down periodically in response to the input current pulse. The input current works as a heat source in this experiment. The current pulse charges the battery in square waveform as shown in Figure 4.1.6. The pulse width of the input current is 180s. The temperature in each test point rose up as shown in the figure. The battery will stop charging in next 180s. So, the temperature will cool down in this period due to losing heat source. The time difference between the kinks of temperature curve and the edge of input current will be measured by comparing the date of

Fig. 4.5. The photo for experimental set-up

current and temperature. The time difference represents the temperature signals lag to response current signal due to propagation of heat flux. Thus, the propagation time of heat between thermal sensors was obtained by comparing the kirks in measured temperature curve to the edge of input current in this experiment.

The propagation delay time can be read from temperature curve and charging current pulse directly. The heat propagation time between center point and surface is 7 seconds on average.

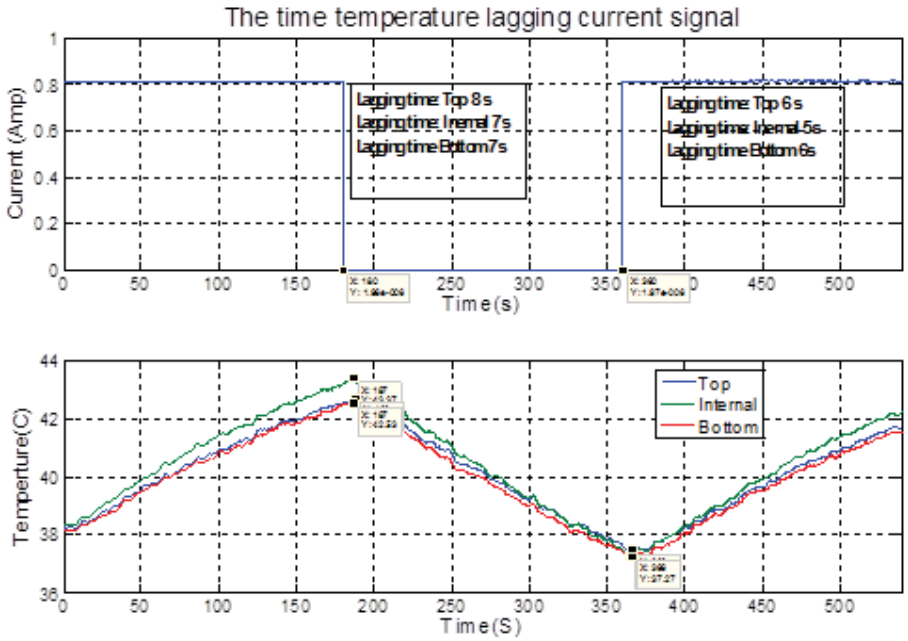

Fig. 4.6. Experimental data for propagation delay test

4.2 Cyclic Constant Current Charge/Discharge Test

As we discussed above, the lithium ion battery need a reference curve of heating power in normal operating condition to adjudge the thermal system errors. To obtain this reference curve, we must design a series of experiments to find the heating power as a function of input current, SOC and ambient.

According to the simplified model, the four parameters are required. Therefore, the experimental tests should be designed to find the parameters. And, we also need to find the lookup table which shows the relationship between output of heating power and TDIS, and the input parameter of current, ambient temperature and SOC. To find the parameters and validate the model, the lithium ion battery should be tested in different current rate and different ambient temperature. If the SOC and heating power can be calculated by the temperature data, the heating power of the battery can be represented as the function of current, SOC and ambient temperature. So, the

standard heating power in the process of charging/discharging can be represented as a lookup table in which the heating power of battery can be found as a function of current rate, SOC and ambient temperature in normal operating condition.

The experimental setup and circuits used are the same as in the propagation delay test. In this test, a modified battery is charged and discharged at certain current rate. The internal and surface temperature is also measured at one time and recorded by Solartron cell tester. The charging/discharging cycle was setup as in Figure 4.7. In this test, the battery is full charged and full discharged in constant current rate at 0.9C, 0.8C, 0.7C, 0.6C, 0.5C, 0.4C and 0.3C. the full charge voltage is set at 4.2V. the full discharge voltege is set at 2.75V. the current and voltage profiles can be read in Figure 4.7.

At one time, the corresponding temperature in internal and surface is also recorded by Solartron cell test. Figure 4.8 shows the temperature change in terms of current rate over time. In the test, the battery was heated up and cooled down periodically in response to the input current turning on or turning off. The parameters in the model will be estimated using with the obtained temperature data in next chapter. The reference of heating power is also made by the temperature and current data in a lookup table.

4.3 Thermal Runaway Test

The detector should be able to detect thermal problems before it happens. In order to verify the detector, some scenarios of failure mode should be designed to validate net effects of TDIS failure detector. In thermal failures in a lithium ion battery, the thermal runway is one of the worst cases to damage the battery. So, in this experiment, a thermal runway will be created to validate the TDIS detector by observing the parameters in the process of battery damaging.

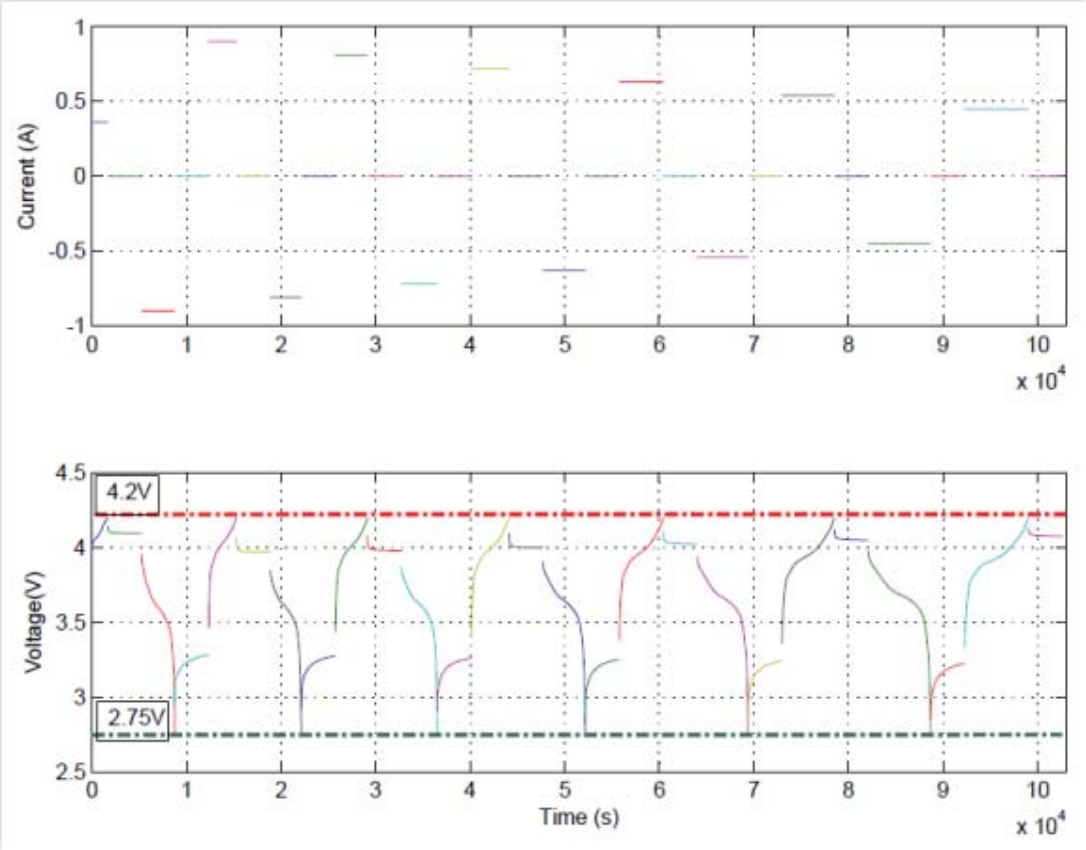

Fig. 4.7. Current setup in constant current cyclic charge/discharge test

4.3.1 Sample Preparation and Test Setup

The experimental set-up and circuit are the same as in the propagation delay test shown in Figure 4.4 and Figure 4.5. A Solartron 1740E with auxiliary temperature measurement is employed to get thermal runaway data which include internal temperature, surface temperature, battery current and battery voltage. The connection of test can be referred to Figure 4.4. However, the test pack needs special process to trigger the thermal runaway. As we discussed before, the thermal runway will happen in case of increasing exothermic reaction and slow heat escape rate. Therefore, the test sample should be designed to fulfill the requirement of thermal runaway occur-

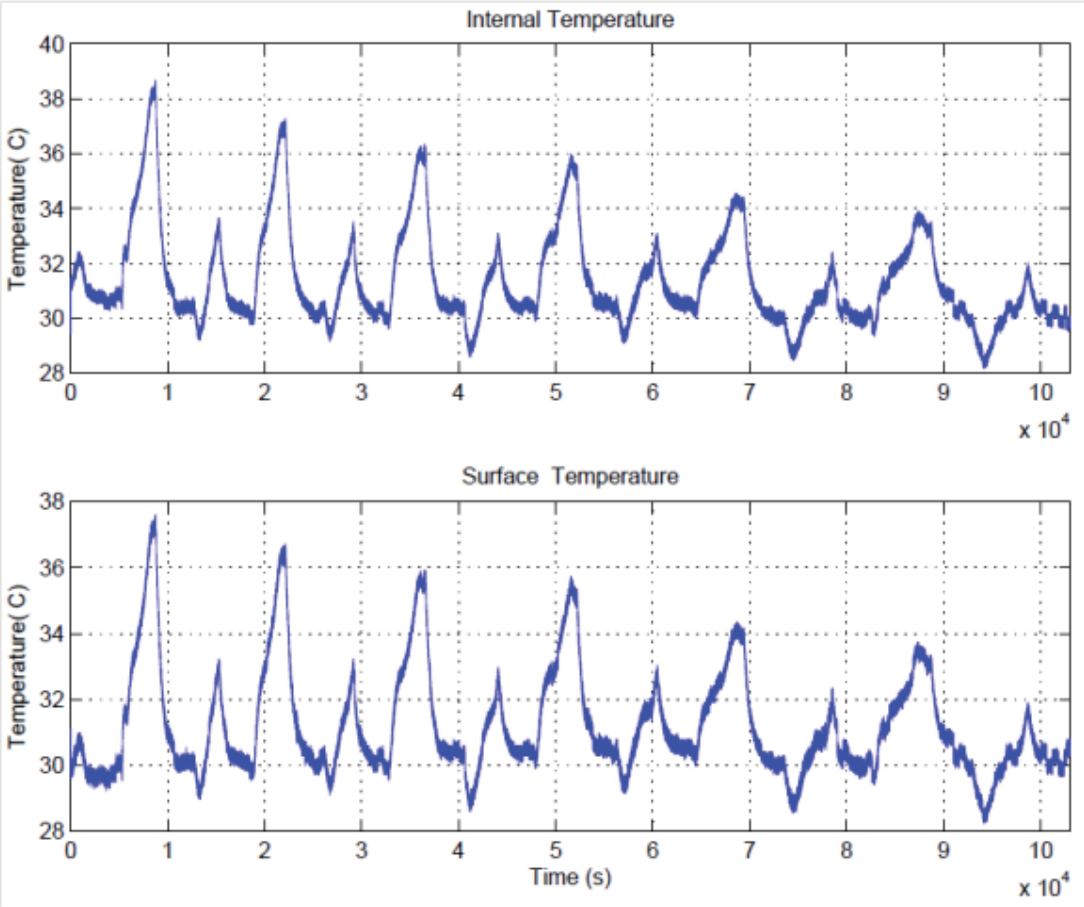

Fig. 4.8. Internal and surface temperature data in the test

ring. To increase the internal exothermic reaction, an internal short circuit should be made to make a high temperature spot in battery. The battery also is covered by diabetic layer to reduce the heat dissipating rate. The test pack is designed as shown in Figure 4.9. The battery is wrapped by glass fiber cotton and aluminum foil to reduce the heat escape rate. A needle with a small hook on the tip is used for short circuit trigger in this test. The test assembly is connected to Solartron cell tester to run a cyclic charging/discharging test. The test assembly is put in an enclosed safety chamber to protect other devices from fire and explosion in the test. The current,

voltage, internal temperature and surface temperature are recorded and will used for analyzing the process of thermal runaway.

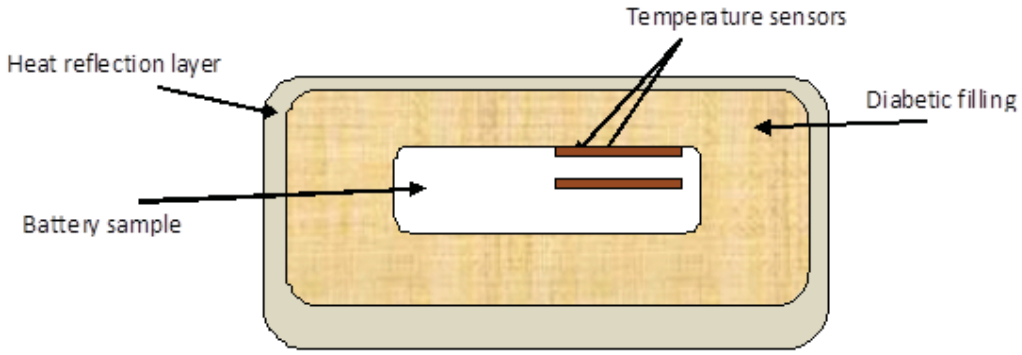

Fig. 4.9. The sample for thermal runaway test

4.3.2 Test Results in Thermal Runaway Test

The photos in Figure 4.10 show the damaged battery after thermal runaway test. The left photo shows the sample assembly after the thermal runway. We can see the wire outlet has been burned by high temperature. The right photo shows the damage in the lithium ion due to the high temperature in the process of thermal runaway. Figure 4.12 shows the temperature change in the process of thermal runaway. The temperature inside the battery can be increased up to 800 °C in seconds. Therefore, the aftermath of thermal runway is catastrophic. The detection for thermal runway is necessary to protect the lithium ion batterers.

4.4 Thermal Capacity Test

In the simplified model, many parameters need to be determined to build practical failure detectors. In this test, the thermal capacity will be found by measuring in

Fig. 4.10. The catastrophic results after thermal runway happened

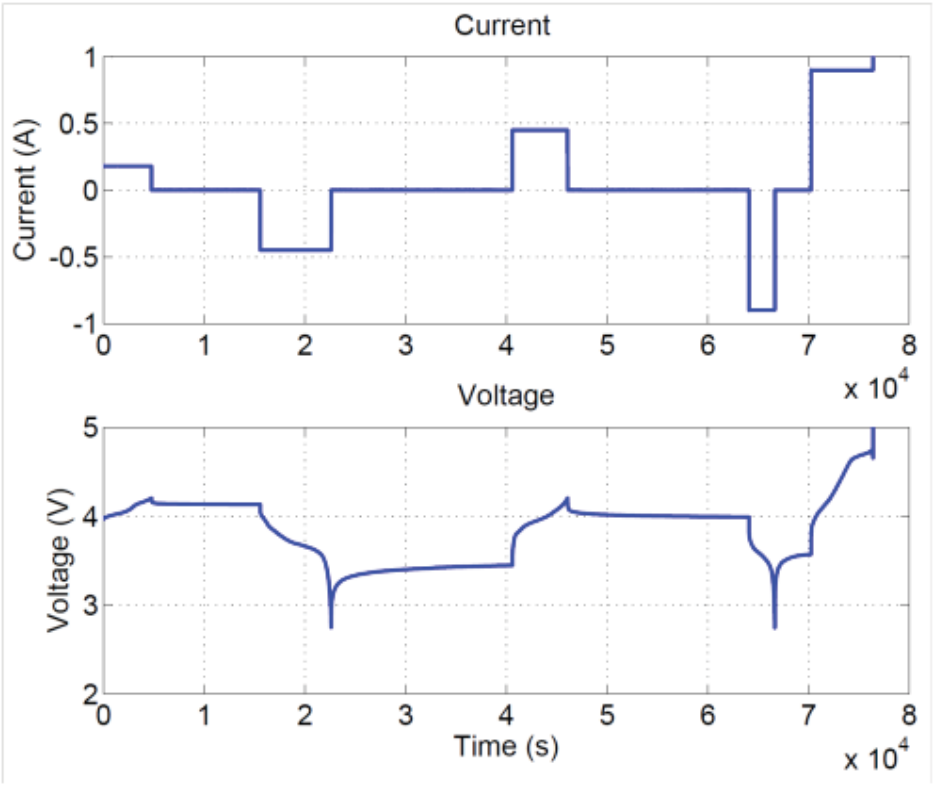

Fig. 4.11. The current and voltage in thermal runway test

comparing to a reference of aluminum block in similar shape, heating power and surrounding condition.

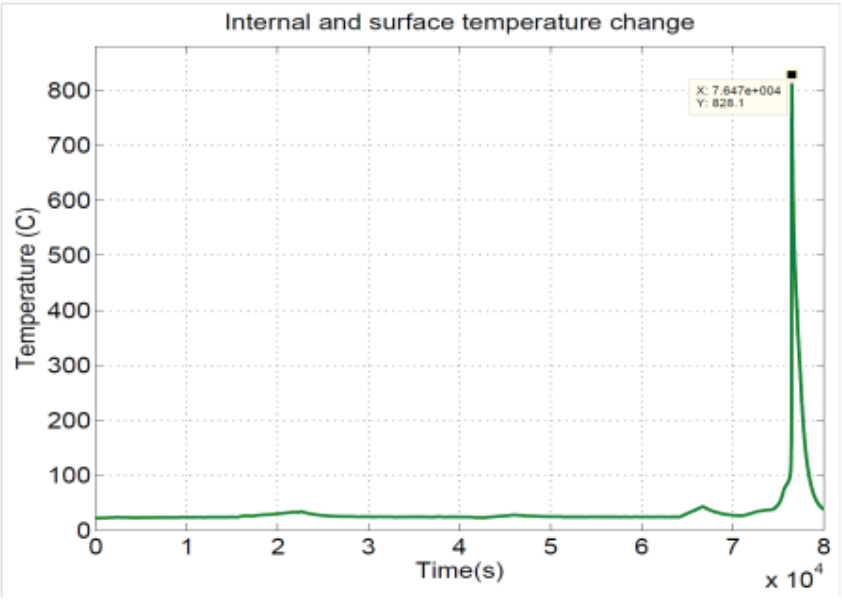

Fig. 4.12. The temperature change in the process of thermal runaway

4.4.1 Test Setup

The test setup is shown in Figure 4.13. In this test, the data acquisition and heat power are both from a Solartron 1470E Cell Tester. The tester provides heating voltage and records the temperature signal in the process of sample heating up. A voltage meter is used to monitor the heating voltage as well. The safety chamber protects the experimenter from the risk of burn, explosion or chemical hazard.

Figure 4.14 shows the sample pack in this test. As shown in the picture, the battery under test is surrounded by adiabatic layer to stop the heat escaping. A thermal couple and a heating pad are stuck to top surface and bottom surface respectively. The thermal couple is used for measuring the temperature of sample and the heating pad is used for heating up the sample in the test. The whole sample pack is covered by heat reflective foil to reduce the heat dissipation further.

Figure 4.15 shows the test circuit for this test. The heater receives a constant voltage from the Solartron Tester to heat up the sample. The voltage and current are

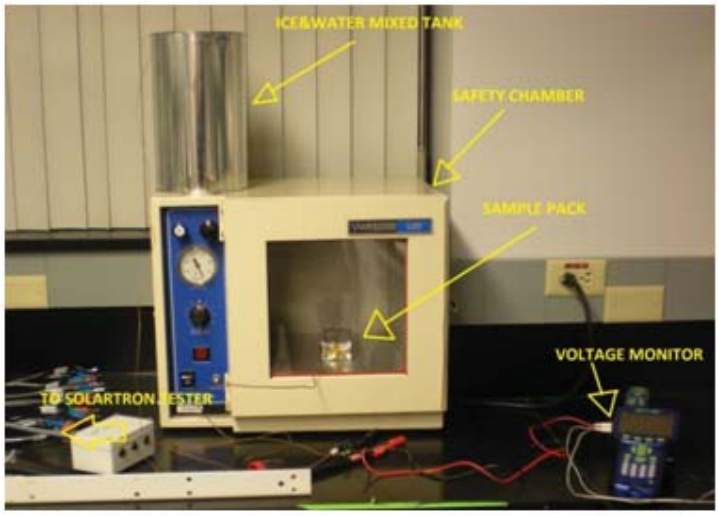

Fig. 4.13. Test setup for thermal capacity test

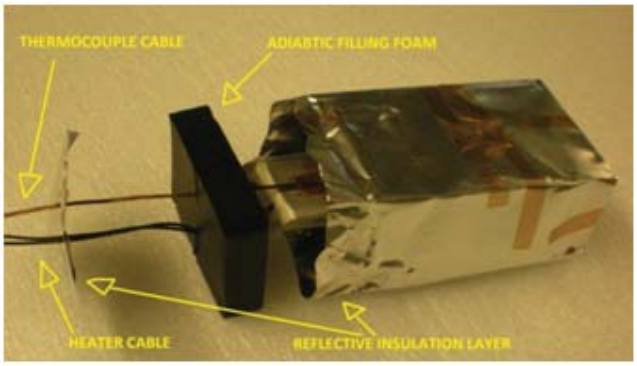

Fig. 4.14. The sample pack in thermal capacity test

recorded by the tester for calculating the heating power. At one time, the temperature change is also recorded by the tester. The thermal capacity will be calculated by comparing the temperature rising rate to the standard aluminum reference.

4.4.2 Testing of Thermal Capacity Test

The test procedure for thermal capacity test is as follows.

• Make an adiabatic pack according the shape and size of aluminum block.

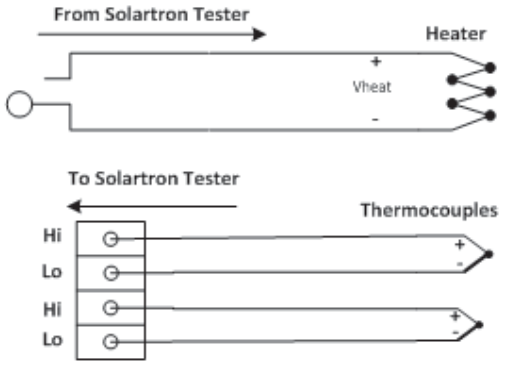

Fig. 4.15. The test circuit for thermal capacity test

• Stick the heating pad to the bottom of aluminum block and attack a thermocouple on the top of the block with Kapton tape.

• Put the aluminum block in the adiabatic pack. And put the pack into safety chamber. Then, connect the thermocouple to auxiliary channel and connect heating pad to a FRA channel.

• Setup a potentiostatic experiment. Set the voltage to 9.00 volt. Then start the experiment for 200 second.

• Turn off the heating voltage to get the curve of temperature dropping.

• Disassemble the sample pack, replace the aluminum block to a lithium-ion battery.

• Put the lithium ion battery in the adiabatic pack. And put the pack into safety chamber. Then, connect the thermocouple to auxiliary channel and connect heating pad to a FRA channel.

• Setup a potentiostatic experiment. Set the voltage to 9.00 volt. Then start the experiment for 200 second.

• Turn off the heating voltage to get the curve of temperature dropping.

• Analyze the data to calculate the thermal capacity of the lithium-ion battery.

The test results are shown in Figures 4.16-4.21. Figure 4.16 shows the temperature rising rate in heating up the aluminum block. Figure 4.17 gives the temperature dropping rate of the aluminum block after turn off the heating voltage. Figure 4.18

shows the temperature rising rate in heating up the lithium ion battery sample. Figure 4.19 illustrates the temperature dropping rate of the battery after turn off the heating voltage. Figure 4.20 and Figure 4.21 show the corrected result and linear fitting result for the aluminum block and lithium ion battery respectively.

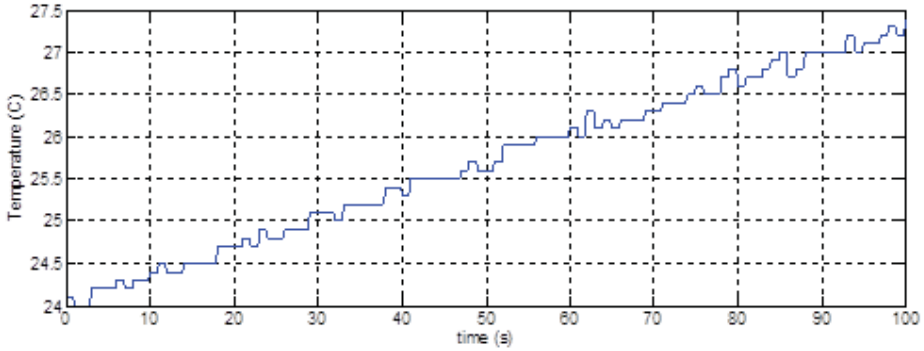

Fig. 4.16. The temperature rising rate result for aluminum block reference

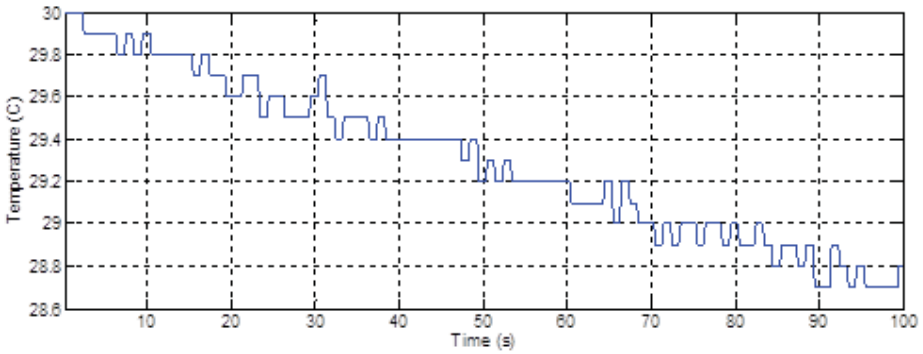

Fig. 4.17. The heat dissipation rate result for aluminum block reference

According to the test results and given parameters, the thermal capacity of the battery can be calculated. The given parameters are shown below. Mass of aluminum block= 23.6761 g Mass of lithium-ion battery = 17.3218 g Thickness of aluminum block = 6.00mm Thickness of lithium-ion battery = 5.8mm Specific thermal capacity of aluminum at 20°C = 879 J/(Kg.°C)

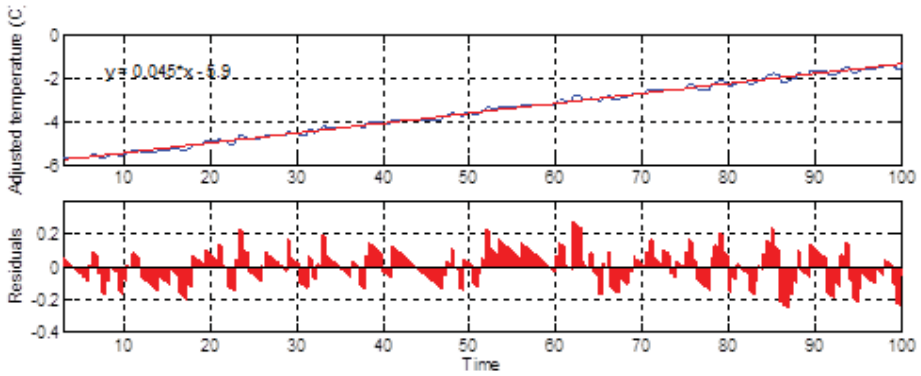

Fig. 4.18. The corrected temperature rising rate and linear fitted curve for aluminum block reference

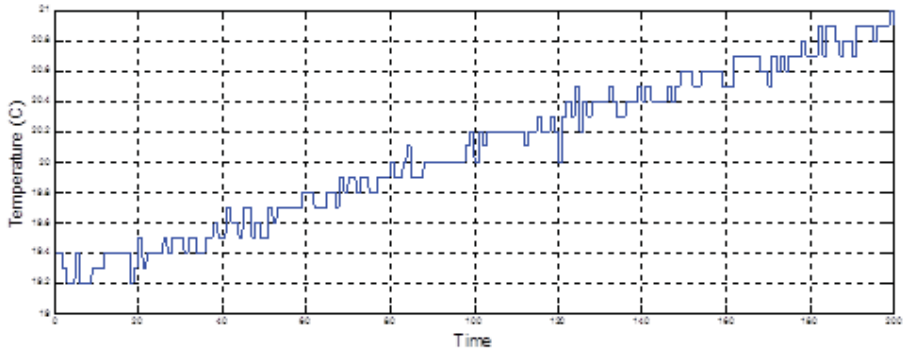

Fig. 4.19. The temperature rising rate result for lithium-ion battery

Thermal conductivity of aluminum = 164W/(m.K) Heating power of aluminum block = 1.029W Heating power of lithium-ion battery = 0.257W The thermal capacity can be calculated by following equations.

$$C_{al} = \frac{P_{al}}{M_{al} \cdot TR_{al}} \tag{4.1}$$

$$C_{ba} = \frac{P_{ba}}{M_{ba} \cdot TR_{ba}} \tag{4.2}$$

The thermal capacity of lithium ion battery should be,

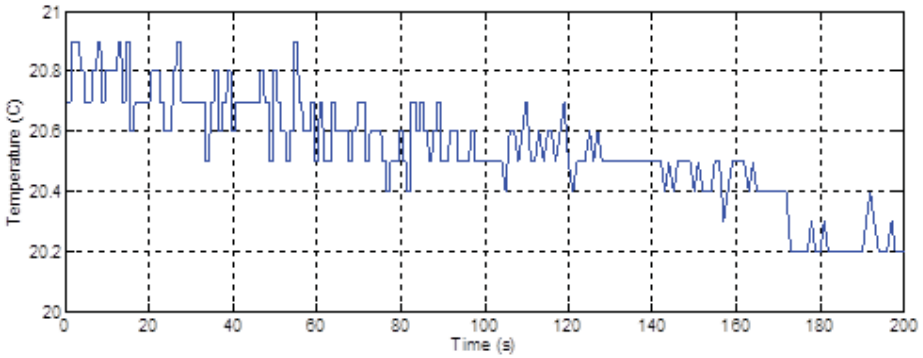

Fig. 4.20. The temperature dissipating rate result for lithium-ion battery

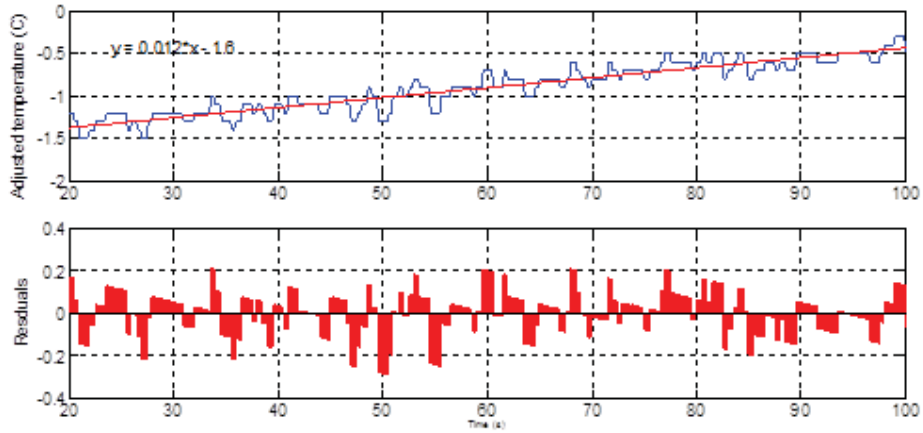

Fig. 4.21. The corrected temperature rising rate and linear fitted curve for lithium-ion battery

$$C_{ba} = \frac{C_{al(P_{ba} * M_{al} * T_{al})}}{P_{al} * M_{ba} * TR_{ba}} \tag{4.3}$$

Where C_{al} is the specific thermal capacity of aluminum block C_{ba} is the specific thermal capacity of lithium-ion battery P_{al} is the heating power of aluminum block P_{ba} is the heating power of lithium-ion battery M_{al} is the mass of aluminum block M_{ba} is the mass of lithium-ion battery TR_{al} is temperature rising rate of aluminum block TR_{ba} is temperature rising rate of lithium-ion battery From the rest results,

the temperature rising rate of aluminum block and lithium-ion battery are respectively $TR_{al} = 0.045$ °C/s $TR_{ba} = 0.012$ °C/s The special thermal capacity is 1126.36 J/Kg.°C. The thermal capacity of the lithium ion battery is 19.51 J/°C.

5. PARAMETER ESTIMATION AND ANALYSIS

In this chapter, the parameters of thermal model will be estimated by analyzing the experimental results from Chapter 4. According to the simplified lumped model, four parameters need to be determined in building the TDIS detector.

• T_d is the propagation delay. It can be measured in propagation delay test.

• C_p, the thermal capacity, which can be abstracted from data of cyclic constant current charging/discharging test.

• Rth_tdis, the thermal resistance between internal point and surface. It can be obtained by analyzing the data of cyclic constant current charging/discharging test.

• Rth_a stands for the thermal resistance between surface and ambient temperature. It can also be analyzing the data of cyclic constant current charging/discharging test.

The estimated parameters will be verified by the data of another cyclic constant current charging/discharging test in Simulink model.

5.1 Parameter Estimation

As explained above, the parameters for thermal model need to be determined by experimental data in normal operating condition in order to build practical failure detector. Except the thermal capacity C_p which has been measured in experiments, the thermal resistance between internal point and surface, and the thermal resistance between surface and surrounding air are also needed to be determined for thermal model. The reference heating power curve is required to adjudge the failure conditions as well. The thermal resistance and normal heating power curve will be obtained next.

5.1.1 Thermal Parameters Estimation by Natural Cooling Process

To estimate the parameters in the simplified lumped model, we need a relatively stable heating power as an input of this model. However, the heating power is variable in the process of charging or discharging. Apparently, the heating power from charging/discharging process is not suitable for estimate the thermal parameters. But, in the naturally cooling process, the input heating power is zero. The only heat released to surrounding air by thermal model is the heat stored in lithium ion batteries. The process of heat transferring can be regarded as the discharging of capacitor through resistors in electrical circuit equivalently. So, we can get the parameters using the capacitance calculation based on an equivalent capacitor-resistor circuit.

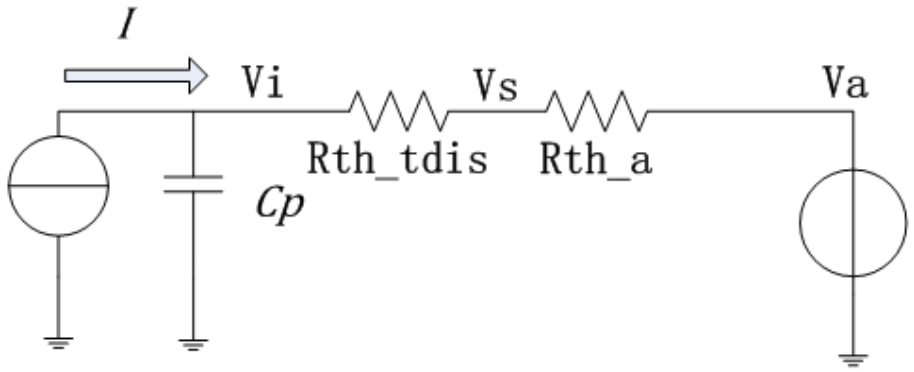

Fig. 5.1. Equivalent circuit for simplified lumped thermal model

Where, the Vi, Vs and Va stand for internal temperature, surface temperature and ambient temperature in voltages respectively. I stand for the heating power Q. And C_p represents the thermal capacity of the lithium ion battery. Thus, the thermal model is represented as an equivalent electrical circuit. The natural cooling process can be analyzed by using the methods in capacitor discharging process analysis. The following figure shows the equivalent electrical circuit of thermal model in natural cooling process.

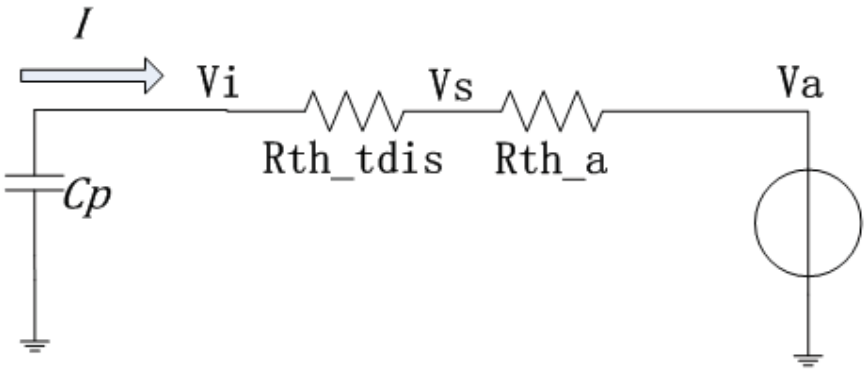

Fig. 5.2. Equivalent circuit for natural cooling process

Because the ambient temperature is constant in the cyclic charging/discharging test, the circuit will be further simplified if the ambient temperature is set as the zero reference point. Thus, this circuit can be simplified as the model shown in Figure 5.3.

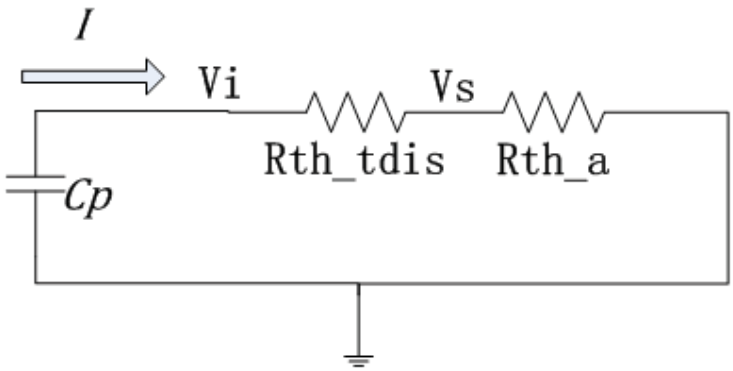

Fig. 5.3. Simplified equivalent circuit for natural cooling process

Where, Vi is the relative voltage of the capacitor referring to Va. Vs is the relative voltage of the capacitor referring to Va I is the current of capacitor which represent the power of heat releasing to airp C_p is the capacitance of the capacitor Rth_tdis is the resistance which represents the thermal resistance of TDIS Rth_a is the resistance which represents the thermal resistance between surface and air

5.1.2 Thermal Parameters Estimation by Curve Fitting

Because the heating power is zero in natural cooling process, it can be regarded as the process of capacitor discharging equivalently. As we know, the capacitor discharging voltage can be described as the following equation (5.1) if the end discharge voltage is zero. In this equation, V0 is the initial voltage of discharging. R*C is the time constant which determine the discharging time. The V0 and R*C can be read by fitting exponential curve if we have the discharge curve of the capacitor.

$$V = V0 * \exp(-\frac{t}{R * C}) \tag{5.1}$$

The following figure shows the typical internal and surface temperature in the natural cooling process in cyclic charging/discharging experiments.

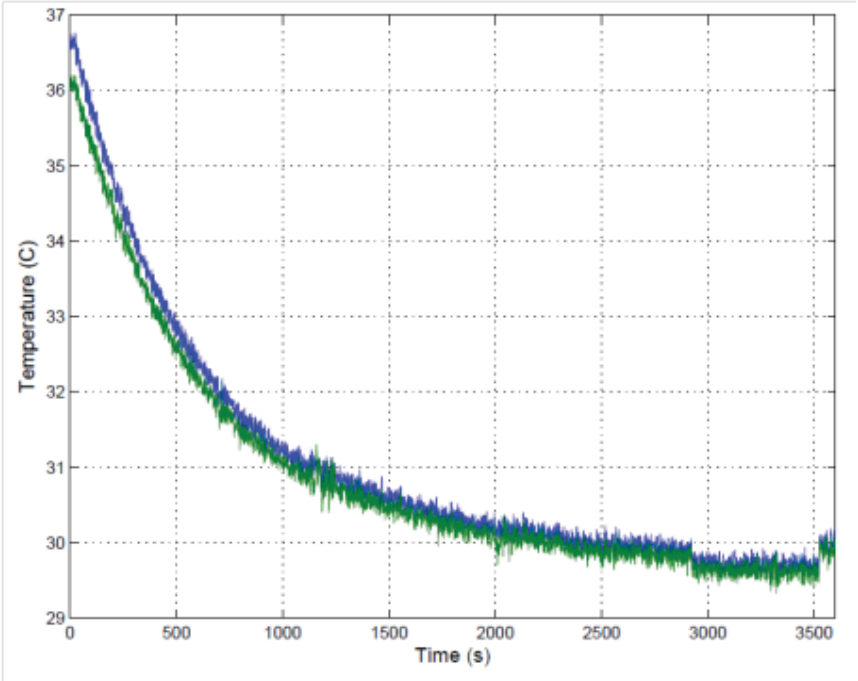

Fig. 5.4. Internal and surface temperature in nature cooling process

In Figure 5.4, the internal and surface temperature was sampled at the ambient temperature 29.81°C. The heated battery has been cooled for an hour after discharged

at current rate 0.81A. The temperature will be subtracted by ambient temperature to fit the equivalent circuit which shown in Figure 5.5. The processed data and the fitted results by Curve Fitting Tools in Matlab are shown as follows,

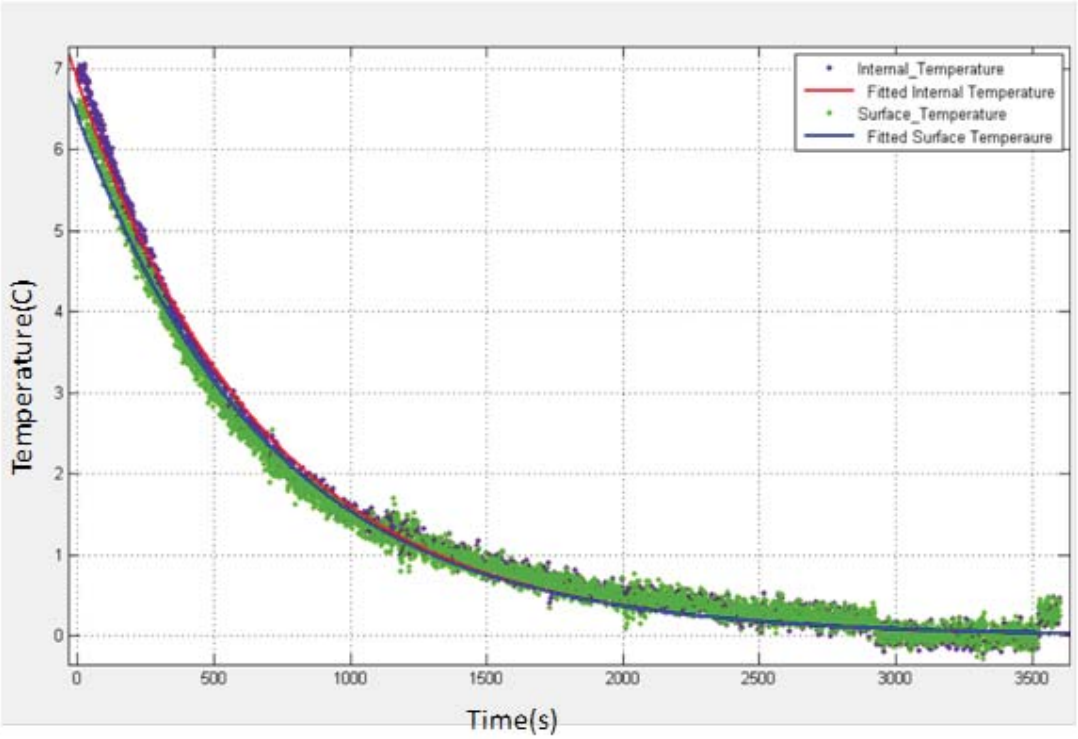

Fig. 5.5. The fitted internal and surface temperature using Matlab Curve Fitting ToolBox

For the internal temperature, the fitted equation is,

$$Vi = 7.135e^{-0.00167t} \tag{5.2}$$

For the surface temperature, the fitted equation is,

$$Vs = 6.716e^{-0.00165t} \tag{5.3}$$

Comparing to Equation (5.1), for internal temperature, we have,

Vi0 =7.135

R*C =1/0.00167=598.878s

For surface temperature,

Vs0 =6.716

Where, R represents the total resistance between capacitor output and ground. Namely, $R = Rth\_tdis + Rth\_a$.

With given C =Cp= 19.51 J/°C.

$R = Rth\_tdis + Rth\_a$ =598.878/19.51= 30.696°C/W

Vs is the output of voltage divider Rth_tdis and Rth_a. So, the relation between Rth_tdis, Rth_a and Vi, Vs can be represented as,

$$\frac{Vi - Vs}{Vi} = \frac{Rth\_tdis}{Rth\_tdis + Rth\_a} \tag{5.4}$$

So, the Rth_tdis should be,

$$Rth\_tdis = \frac{Vi - Vs}{Vi}(Rth\_tdis + Rth\_a) = \frac{Vi0 - Vs0}{Vi0}(Rth\_tdis + Rth\_a) \tag{5.5}$$

Rth_tdis = (7.135-6.716)*/7.135 = 1.8 °C/W Rth_a =30.696 -1.8 = 28.89 °C/W

Thus, we have the C_p = 19.51J/°C and Rth_tdis = 1.8 °C/W in normal operating condition by fitting natural cooling process.

5.1.3 Heating Power Calculation by Direct Measurement

To judge the failure of the lithium ion battery, a standard heating power reference is required. To obtain the standard heating power reference, we need get series of heating power curve based on input current and SOC in normal operation condition. In this section, the standard heating power reference will be calculated by the data in cyclic constant current charging/discharging experiment and the parameters from last section. As we discussed before, the heating power can be calculated by the internal

temperature rising rate and the TDIS if the C_p and Rth_tdis are known. According to Equation 3.12 and given Rth_tdis and C_p, the total heating power in a lithium ion battery can be represented as,

$$Q = \frac{TDIS}{Rth\_tdis} + C_p\frac{\partial T_i}{\partial t} = \frac{TDIS}{1.8} + 19.51 * \frac{\partial T_i}{\partial t} \tag{5.6}$$

or

$$Q = \frac{TDIS}{Rth\_tdis} + C_p\frac{\partial T_i}{\partial t} = \frac{Ti - Ta}{30.696} + 19.51 * \frac{\partial T_i}{\partial t} \tag{5.7}$$

Rth_tdis = (7.135-6.716)*/7.135 = 1.8 °C/W Rth_a =30.696 -1.8 = 28.89 °C/W Thus, we have the C_p = 19.51J/°C and Rth_tdis = 1.8 °C/W in normal operating condition by fitting natural cooling process.

5.1.4 The Heating Power Reference Based on Current and SOC

To detect the failure of the lithium ion battery, a standard heating power reference is required. In this section, the heating power in normal condition will be calculated under current rate and SOC. The heating power curve will be used as a standard to judge thermal runaway in next chapter. The SOC is calculated by the integration of current as the following equation. In charging process,

$$SOC = (\frac{1}{C}) * \int Idt \tag{5.8}$$

In discharging process,

$$SOC = 1 - (\frac{1}{C}) * \int Idt \tag{5.9}$$

Where, the C is the capacity of the battery and I is the current Because the battery is charged or discharged in constant current in this test, the SOC can be represented as, In charging process,

$$SOC = I * \frac{t}{C} \tag{5.10}$$

In discharging process,

$$SOC = 1 - I * \frac{t}{C} \tag{5.11}$$

Thus, we will have a two dimension lookup table of heating power with using the current as input,. The table will be used as a reference for TDIS detector.

Figure 5.6 shows internal temperature and surface temperature in 1C discharge rate in a full discharge process.

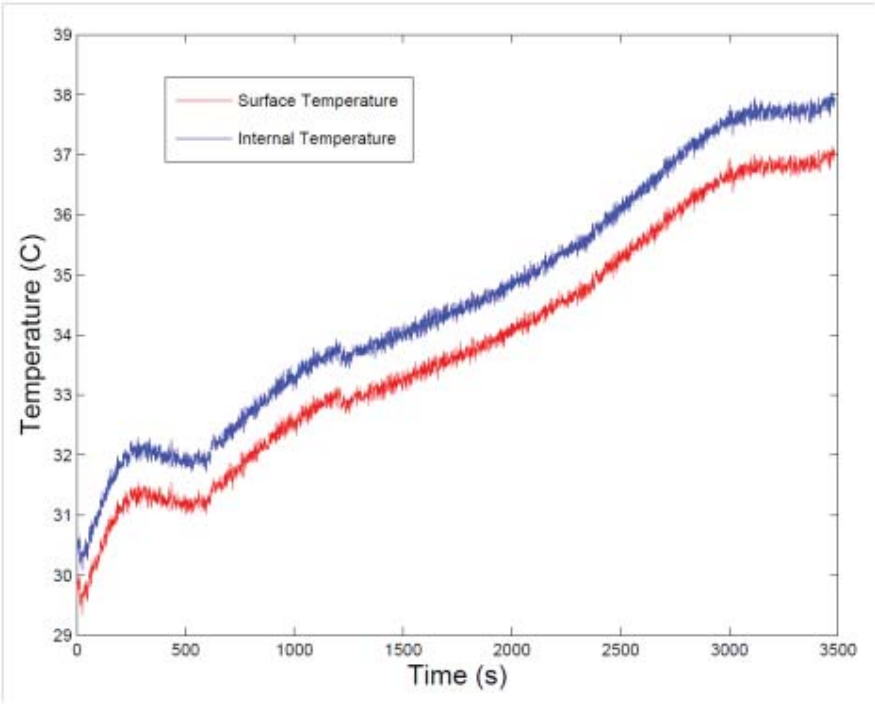

Fig. 5.6. The internal temperature and surface temperature in 1C discharge process

The corresponding heating power by equation 5.6 is shown in follows.

We can see that the heating power in this type of lithium ion battery is variable in the progress of discharging. In the beginning and the end of discharge, the heat is generated relative high. And in period of 0.9 to 0.2 SOC, the heating power increases gradually. So, the risk of over-heat is higher in the beginning and end of discharge

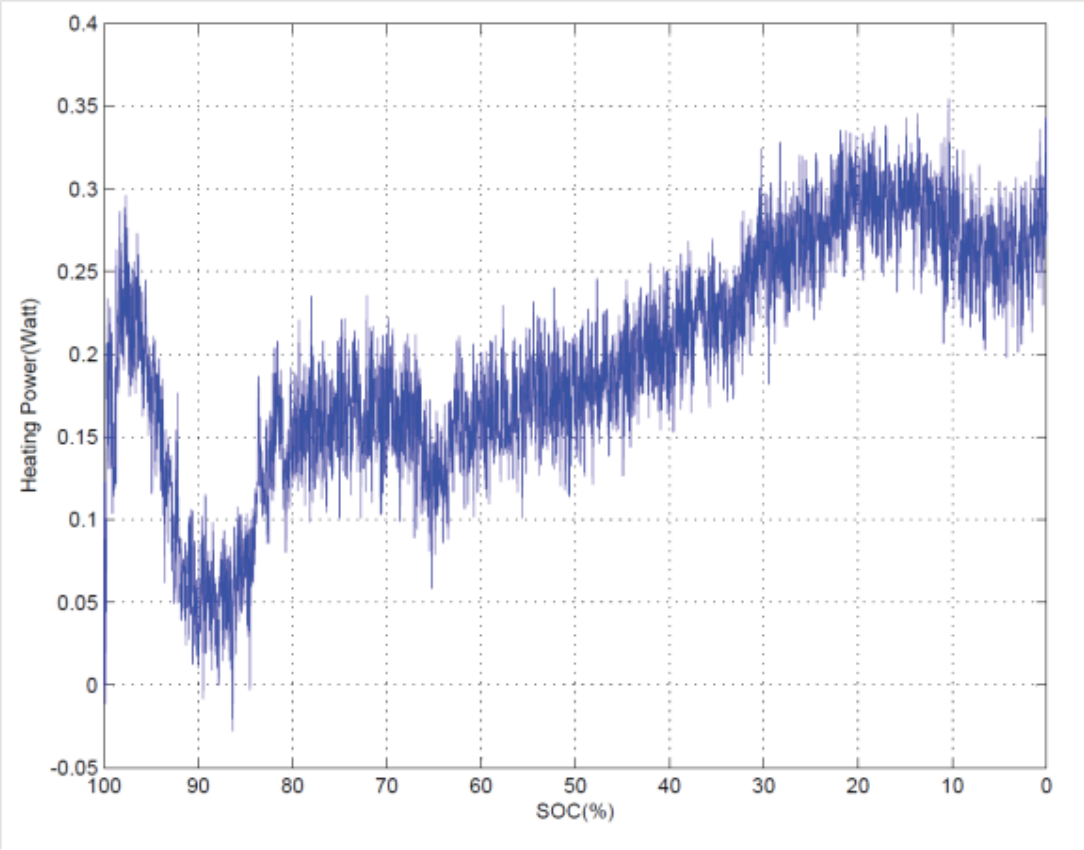

Fig. 5.7. Heating power at 1C current rate in discharging process

according to the curve of heating power. The Figure 5.1.8 shows the heating power curve in 1C current rate in charging process.

The curve of heating power can be obtained in repeating charging/discharging at the rate of 0.5C, 0.6C, 0.7C, 0.8C, 0.9C and 1C. because the heating power at the rate lower than 0.5C is too little to measure accurately according to current experimental setup, the we only study the heating power in current higher than 0.5C in this experiment. Thus, we have a group of data to describe the heat generated in charging and discharging process.

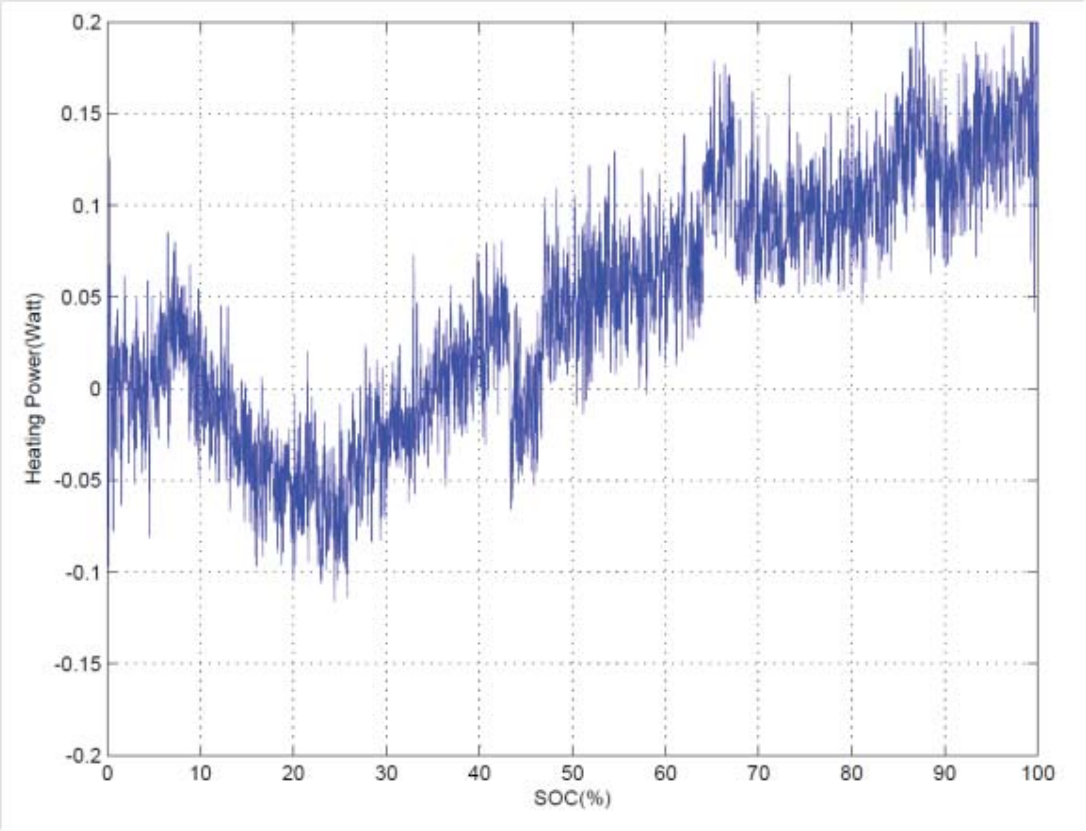

Fig. 5.8. Heating power at 1C current rate in charging process

5.1.5 Look-up Table Simplification by Linear Piecewise Approximation

A practical detector needs high efficiency in on-line calculation. However, the heating power curve we measured in last section is too big to use in practice. A lookup table is required in detector design to represent the relation between heating power, and input current and SOC. We need to develop a look-up table based on the heating power curves which were calculated in last section.

From the heating power curve in last section, because strong noise is existed in the background of the measured temperature signal, the result need be processed by approximation method to smooth the signal and reduce the calculation in look up

heating power. The piecewise linear function is a suitable method due to approximation.

The simplified lookup table for heating power of lithium batteries in normal operating condition is shown in Table 5.1 and Table 5.2 respectively. The Table 5.1 shows the heating power in discharging process with SOC from 100 to 1 in different current rate. The Table 5.2 shows the heating power in charging process with SOC from 1 to 100 in different current rate. The heating power between -0.5 C current rates and 0.5 C current rate is too little to ignore. The heating power in this range can be regarded as zero in calculation.

5.1.6 Verification of Heating Power Reference

The model parameters and lookup table of heating power will be verified by simulation results in this section. To validate the hearing power in Table 5.1, an experimental data at 0.9C discharging rate is used for comparison. The heating power in the look-up table is used as input. The internal temperature will be calculated by Equation 5.6. Figure 5.7 shows the calculation result of internal temperature and the experimental data.

According to above figure, the calculation results match the experimental result approximately. In the beginning period, the temperature has the error as much as 0.8°C. This mismatch probably results from the fluctuation of ambient temperature in the process of experiment. Because the simulated internal temperature is calculated base on fixed ambient temperature, an error can be made by the variable ambient temperature.

The error reduced over time, the calculated results and experimental data fit better. At the end of discharging, the estimated temperature matches the experimental perfectly. It indicates that the equation and look-up table are effective in estimating temperatures in the simple lumped model in normal operating condition.

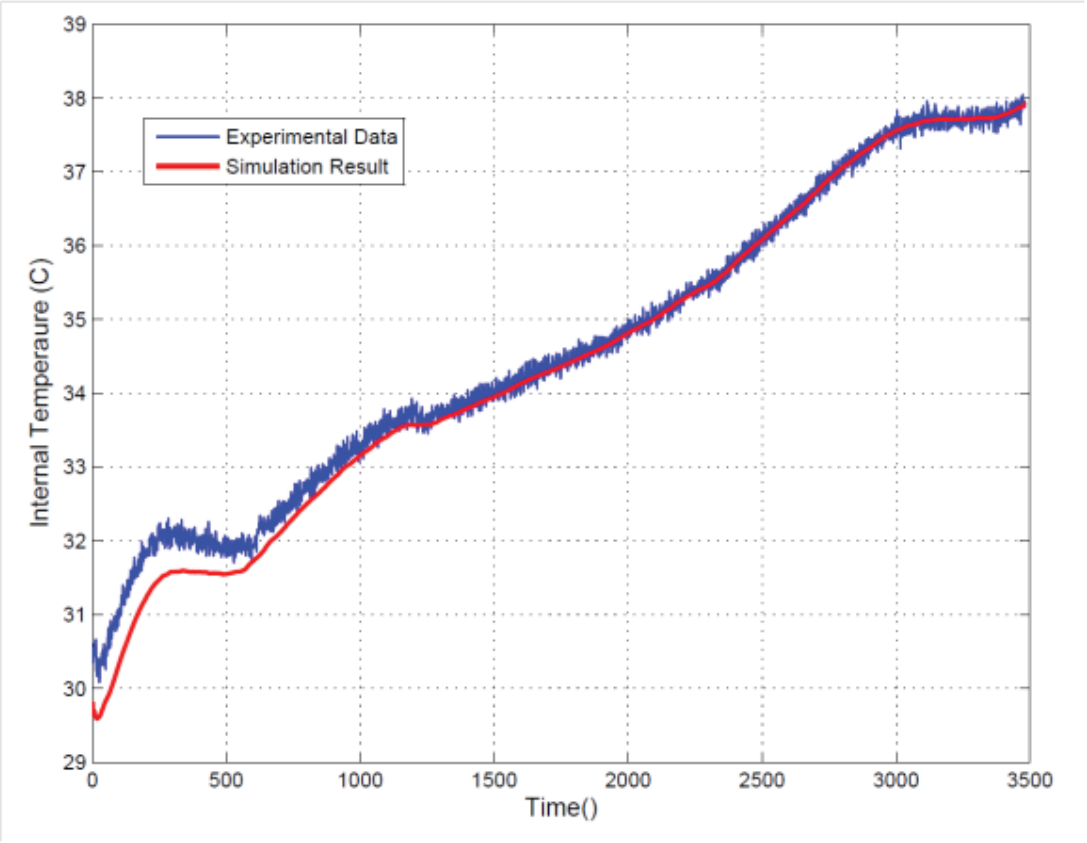

Fig. 5.9. Comparison of estimated of internal temperature and experimental data

6. DETECTOR DESIGN AND VALIDATION

As we discussed before, the thermal runway occurs under two conditions - the increasing heating power and poor heat dissipation. Therefore, the detector should be designed in detecting abnormal heating power and changed thermal heat escape rate respectively. In this chapter, the heating power detector and TDIS detector will be designed and validated base on the heating power reference and thermal model which from the look-up table and model parameters in Chapter 5. The detectors will be validated by the data of thermal runway as well.

6.1 Heating Power Failure Detector Design

As we discussed in Chapter 3 and Chapter 4, the heating power can affect the battery in two aspects according to simplified lumped model. First, the heat can heat up the battery. The heating power for this part can be represented as $C_p \frac{\partial T_i}{\partial t}$. The C_p is the thermal capacity of the lithium ion battery. Also, some heat will escape to the surrounding. This part of heating power can be represented as $\frac{TDIS}{Rth\_tdis}$. Where, the TDIS and Rth_tdis are the temperature difference between internal point and surface and thermal resistance between internal point and surface. The total heating power can be obtained by adding the two heating powers. That is to say, the heating power can be measured if we know the internal temperature changing rate and TDIS base on the thermal capacity and thermal resistance from Chapter 5.

The following figure shows the structure of the detector.

where, I is the charging/discharging current Ti is temperature at internal point Ts is the temperature on surface SOC is the state of charge ΔTm is the measured TDIS Pref is the heating power reference Pc is the heating power stored by thermal capacity

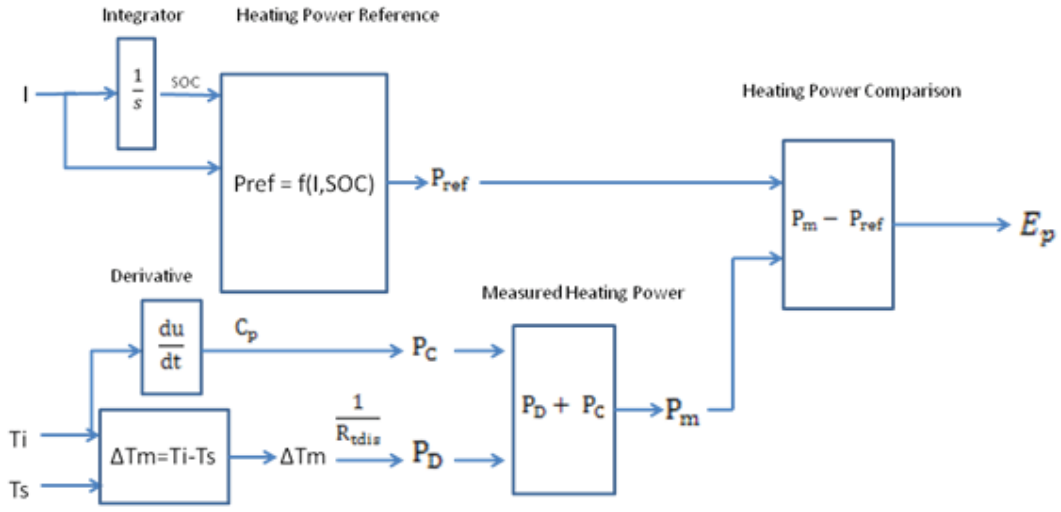

Fig. 6.1. Structure of heating power failure detector

Pd is the heat dissipated to surrounding air Pm is the measured total heating power Ep is the error between measured heating power and reference.

6.2 Thermal Model Failure Detector Design

To detect the failure of battery which results from changed parameters of model, a parameter change detector is needed base on the TDIS model. The detector will be designed as below diagram.

In this detector, the heating power of battery is measured. The measured heating power will be used as an input of thermal model which has the parameters in normal operating condition. If the measured TDIS is much smaller than the output TDIS, the system will be indicated in bad heat dissipation. In other words, the system takes the risk of thermal runaway.

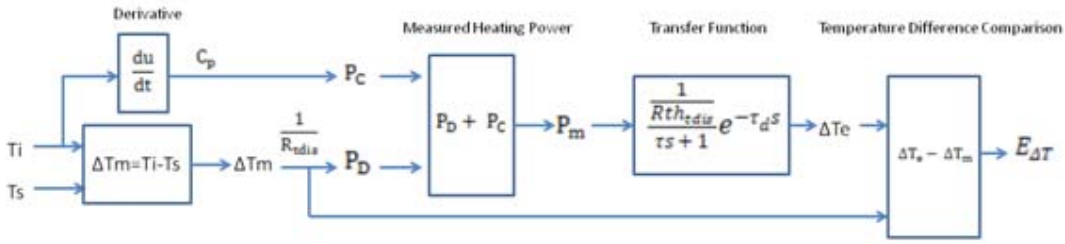

Fig. 6.2. Structure of thermal model failure detector

6.3 TDIS Detector Design

If we combine the two detectors described above, a detector can detect both abnormal heating power and changed thermal parameter at a time. As shown in Figure 6.3, the detector has both output of error of heating power and error of TDIS. This structure will make the detector more flexible and versatile. It can determine two aspects - heat escaping rate and heat accumulation rate which can lead to thermal runaway. The structure of the detector is shown as below diagram.

The detector can detect the failure in two aspects. First, the abnormal heating power generation should be detected by comparing to the heating power reference. Secondly, the abnormal thermal resistance should be detected by comparing to the thermal resistance in normal operating condition. The flow chart of failure detection is shown in Figure 6.4.

The E_p and $E_{\Delta T}$ represent the errors between measured heating power and heating power reference, and measured TDIS to the normal TDIS. The simulation in Matlab/Simulink is shown in Figure 6.5,

6.4 Detector Validation by Thermal Runaway Test

To validate the TDIS detector, we need the data in thermal runway test to detect the abnormal thermal model output and abnormal heat generation. In the process

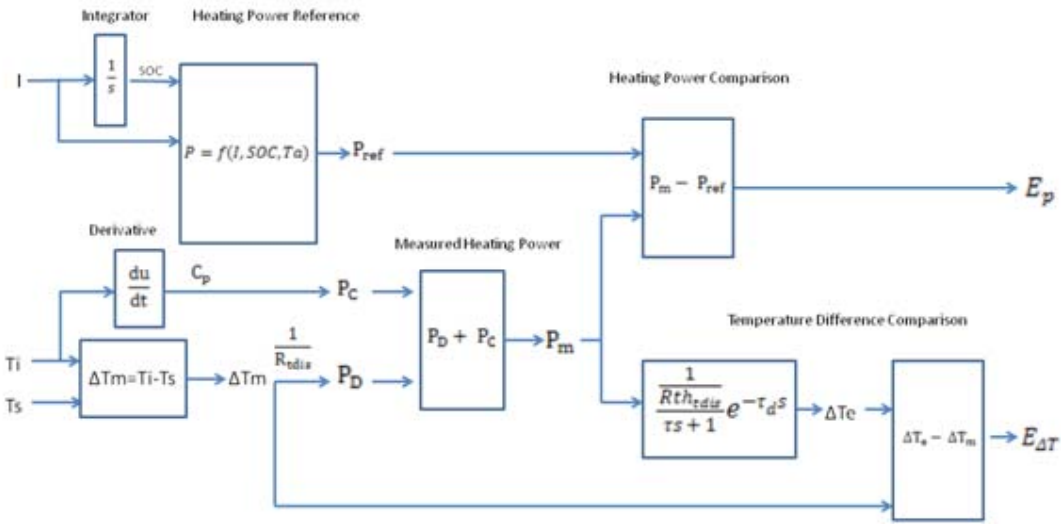

Fig. 6.3. TDIS detector for detecting thermal runaway problem

of thermal runaway, the sample of lithium ion battery is set in poor heat dissipating condition. In other words, the thermal resistance between surface and ambient is very large. If the TDIS detector works well, the abnormal TDIS due to the poor heat dissipation should be detected before thermal runaway and the heating power increase should be detected after thermal runaway occurs.

The temperature change in thermal run away test has already shown in experimental results. To focus on the thermal runaway process in the beginning, we study the experimental data from the one charging/discharging cycle to the onset point of thermal runway. Figure 6.6 shows the current setup in this period.

Figure 6.7 shows the comparison of measured TDIS and calculated results from measured power. Figure 6.8 shows the $E_{\Delta T}$ which output by thermal model failure detector. From the data, the estimated TDIS is much higher than measured TDIS all the time. It is indicated that the system distributes less power to dissipate to the air at the similar heating power. The majority of heating energy is used for increasing

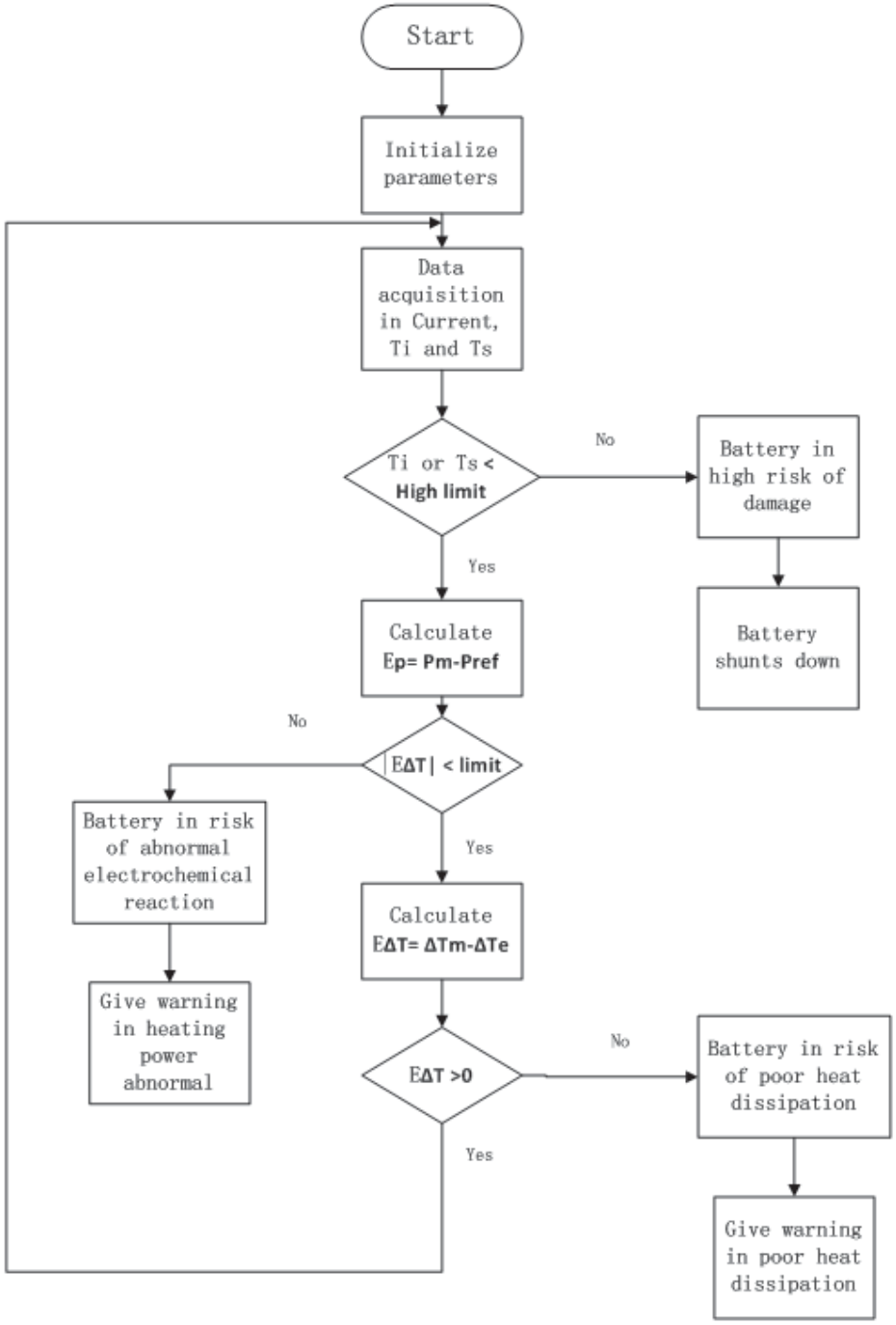

Fig. 6.4. Flow chart of TDIS detector for detecting heating power and thermal model problem

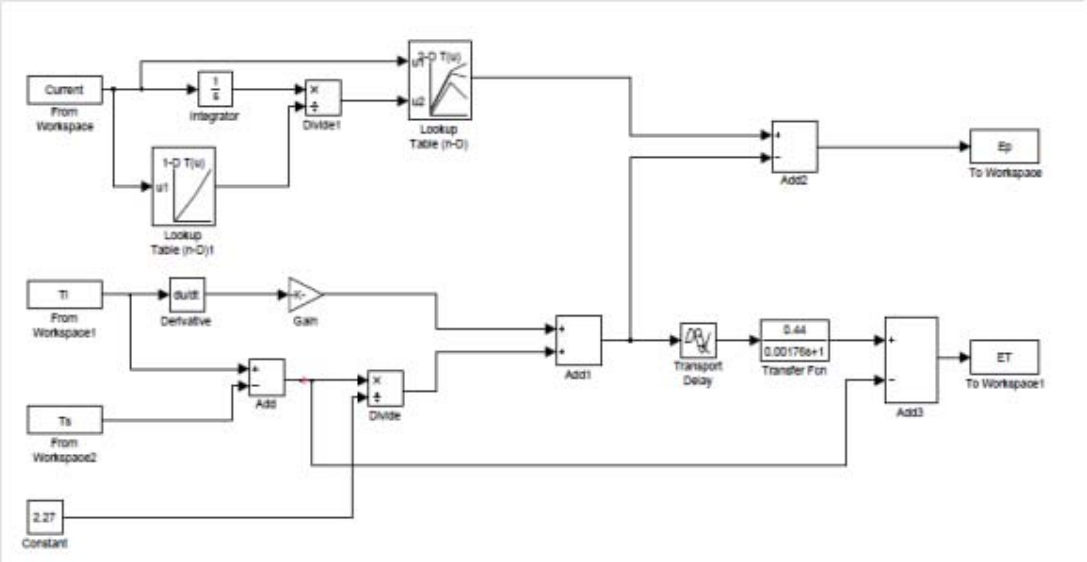

Fig. 6.5. Simulink schematic for TDIS detector

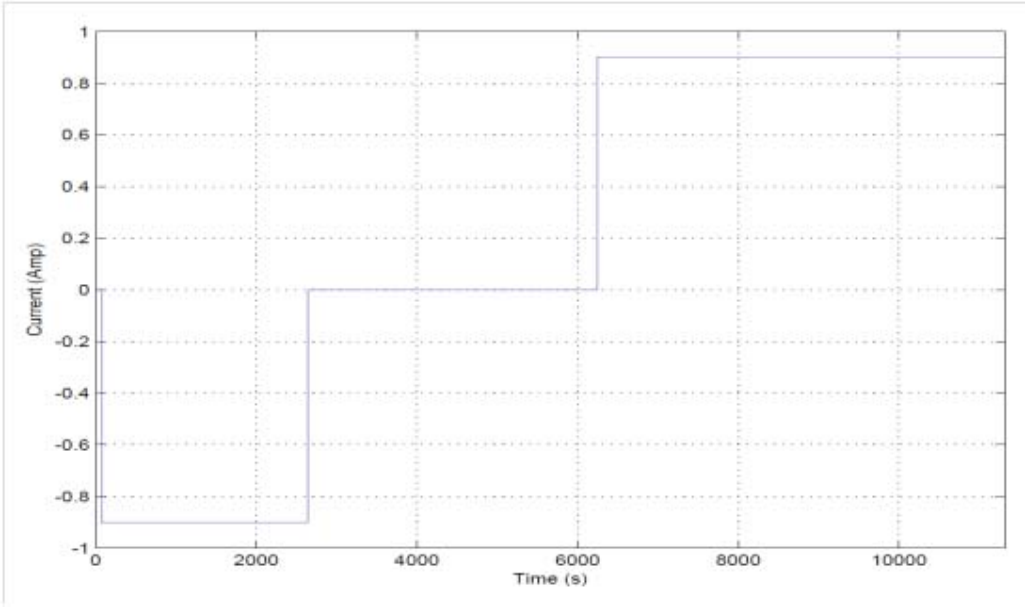

Fig. 6.6. Current charging/discharging setup for thermal runaway test

temperature instead of transferring to surrounding. This illustrates that the thermal system has very poor heat dissipation to lead to thermal runaway.

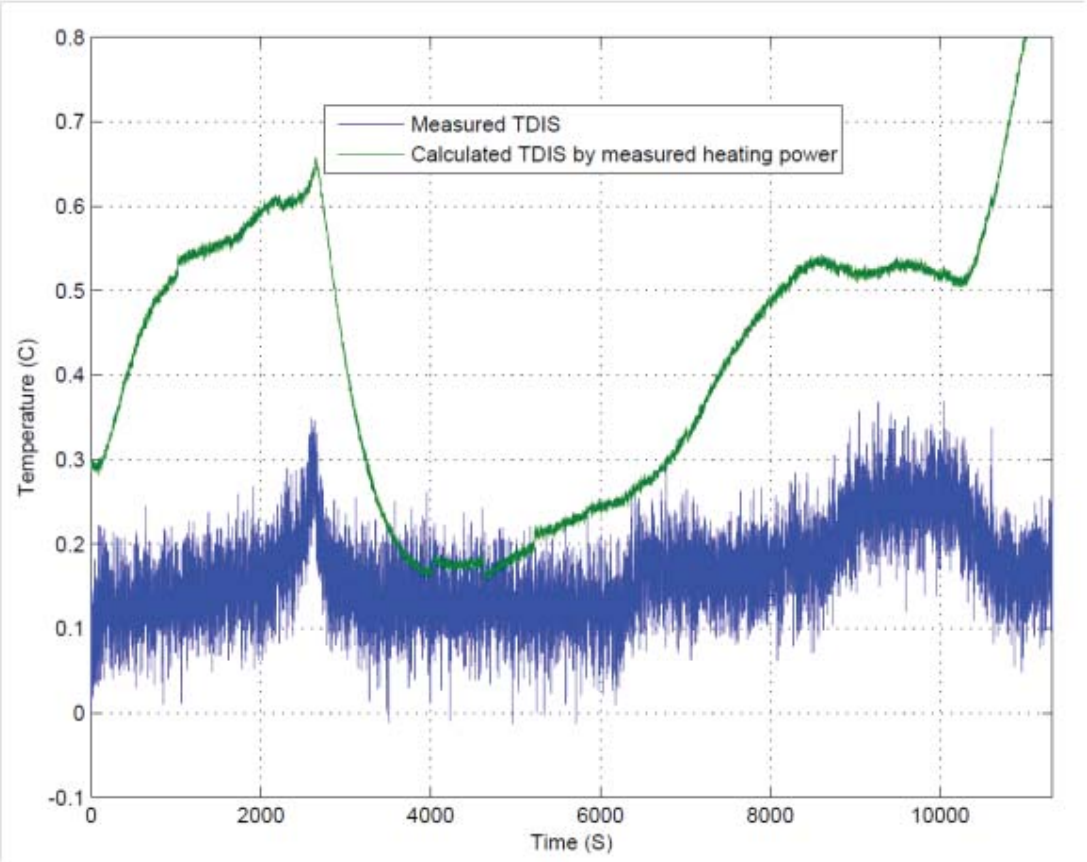

Fig. 6.7. Comparison of TDIS between measured data and calculated results from measured power

Figure 6.9 shows the comparison of estimated heating power and measured heating power. Figure 610 shows the Ep output from abnormal heating power detector.

According to the result, in the first discharging period, the experimental result matches the estimated results perfectly. In the charging process, the heating power starts to offset the estimated curve. At the onset point of thermal runaway, the

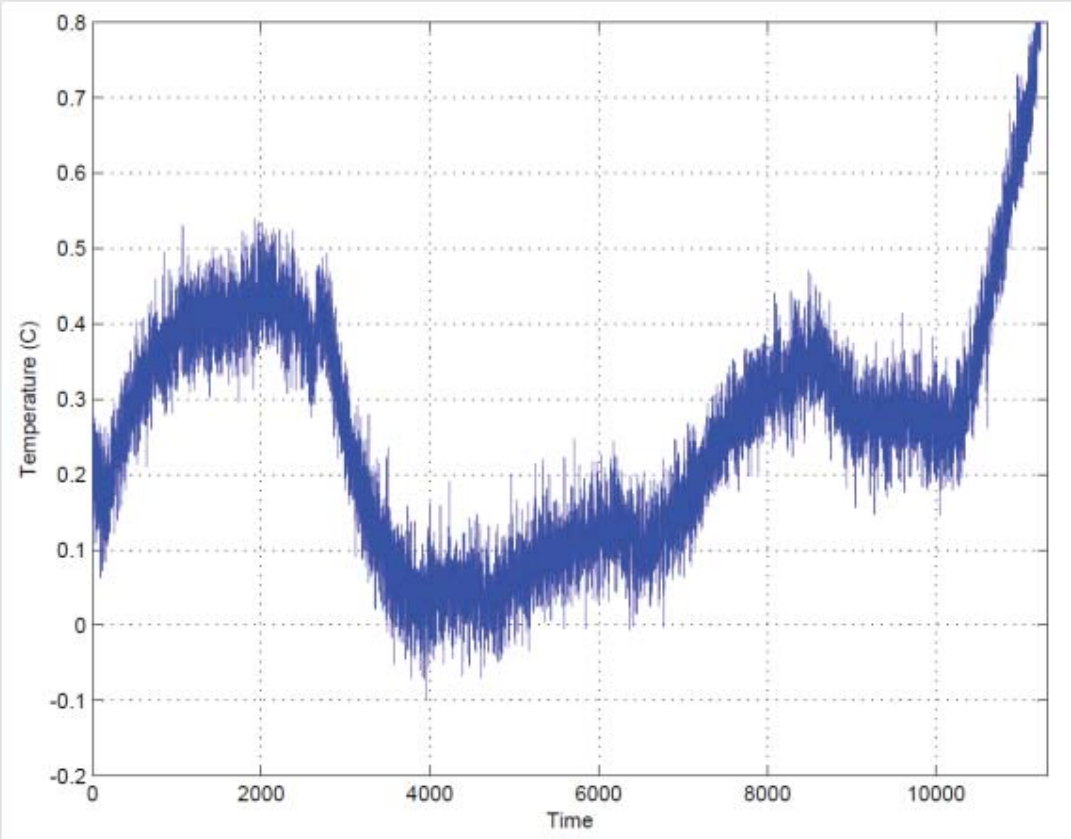

Fig. 6.8. the ET output from thermal model failure detector

heating power increased sharply. The heating power is out of control to result in thermal runway.

From the results of detector output, the TDIS detector can capture the abnormal change based on both thermal model parameters and heating power at least 1 hour before thermal runaway happened in this test. As a proposed method to detect thermal runaway in early time, it works effectively and sensitively.

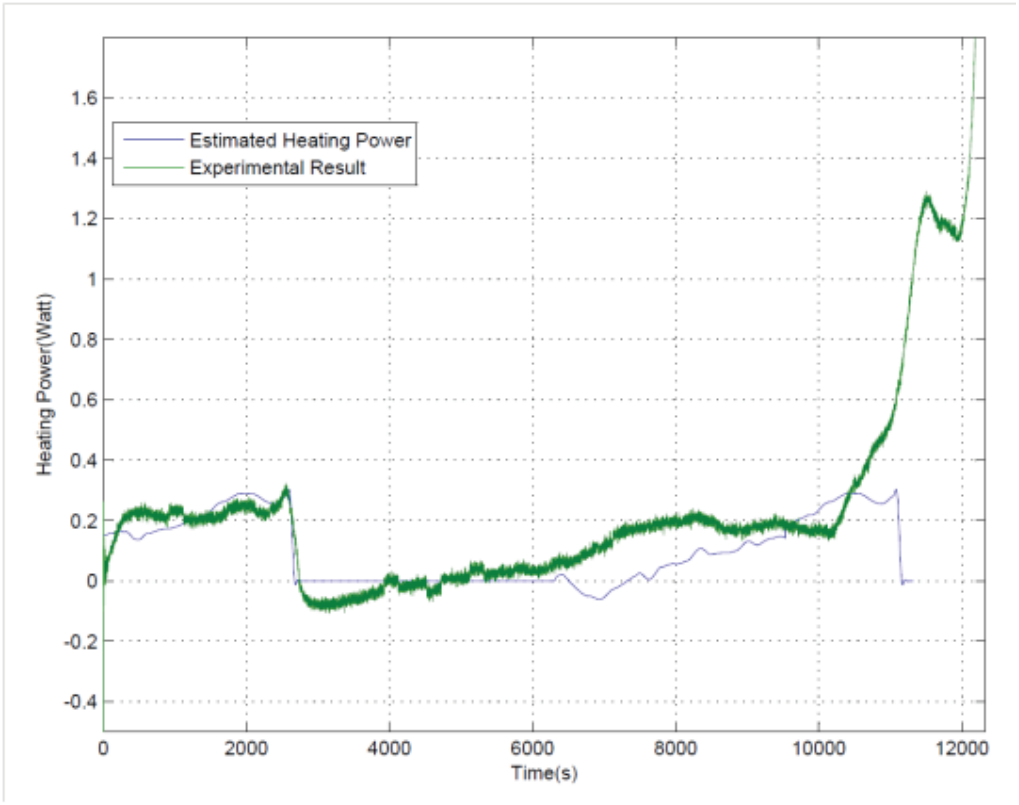

Fig. 6.9. The comparison of estimated heating power to measured heating power

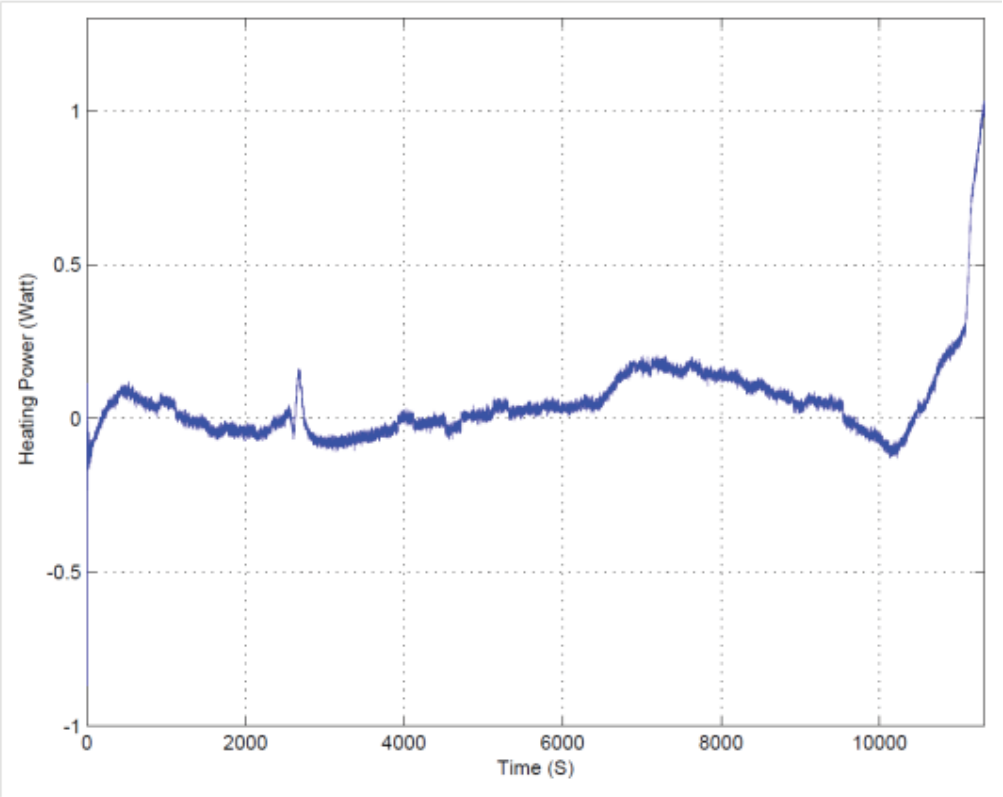

Fig. 6.10. The Ep output from abnormal heating power detector

7. CONCLUSION AND FUTURE WORK

The safety has been one of the most important concerns for the lithium ion batteries due to their unsafely nature. At this concern, a simple, practical and sensitive failure detector was developed in this thesis.

(1) In this thesis, the TDIS has been chosen as a key parameter to develop a simplified model for a designing practical and efficient failure detector. The introduction of TDIS is a key to develop this detector for capturing lithium ion battery failure. The temperature between internal point and surface is more stable and convenient in building model and measuring heating power in generation and propagation than the surface temperature. It gives the detector a relative stable and reliable parameter in measuring heating power and estimating model parameters. The TDIS is validated by experiments as a convenient and appropriate parameter in heating power detection.

(2) A simplified model was build based on TDIS parameter. The simplified model reduced the calculation in designing a real-time failure detector. This lumped simplified thermal model was deducted by the physical law of heat generation and propagation in a prismatic lithium ion battery. This model is simple and efficient to be used for TDIS detector in failure early detection.

(3) Moreover, a failure detector based on TDIS parameter and simplified model is developed to detect either heat generation error or heat propagation error in a prismatic lithium ion battery. The TDIS detector only use charging/discharging current as input, and heating power and TDIS as output to detect battery failure by comparing aberrant heat generation and transportation to the heating power look-up table in normal operating condition.

(4) This detector was validated to detect aberrant heating power in a cycle before thermal runaway happens in thermal runaway test. In experimental tests, the TDIS detector was validated a sensitive and effective detector in lithium ion battery

thermal runway failure detection. In this thermal runway test, the TDIS detector detected the thermal parameter by which the thermal runway can be conducted before charging/discharging cycles of thermal runway happening. The TDIS detected the aberrant heating power before thermal runway in this test as well. The detector also can detect the thermal runway occurring in seconds earlier than the time at which temperature over the temperature limit.

The TDIS method was proved and validated to be effective for lithium ion battery in early failure detection in heating power related catastrophic failure especially the thermal runaway.

In the future, some work will be done to improve the detection according to the drawbacks and the limitation of TDIS detector in this thesis.

• The ambient temperature will be introduced as a new input to make the look-up table more accurate.

• The thermal resistance in the model will be regarded as a variable instead of fixed value to improve the accuracy

• An on-line heating power calculation method needs to be developed instead of look-up table when systematic research about the mechanism of lithium ion battery is clearer.

Hence, we conclude that the proposed model and detector in the thesis is a new progress in the thermal related failure detection for lithium ion batteries. It was proved to be sensitive and effective in the thermal runway detection. However, it still has room to improve to be applied to the model for a more precise and efficient failure detection in early time.

LIST OF REFERENCES

LIST OF REFERENCES

[1] M. Whittingham, "Electrical energy storage and intercalation chemistry.," *Science;(United States)*, vol. 192, 1976.

[2] R. Yazami, "From rome to como: 20 years of active research on carbon-based electrodes for lithium batteries at inp-grenoble," *Journal of Power Sources*, vol. 97, pp. 33–38, 2001.

[3] R. Yazami and P. Touzain, "A reversible graphite-lithium negative electrode for electrochemical generators," *Journal of Power Sources*, vol. 9, pp. 365–371, 1983.

[4] M. Whittingham, "Lithium batteries and cathode materials," *Chem. Rev*, vol. 104, pp. 4271–4302, 2004.

[5] M. Thackeray, "Lithium insertion into manganese spinels," *Materials Research Bulletin*, vol. 18, pp. 461–472, 1983.

[6] G. Nazri and G. Pistoia, *Lithium batteries: science and technology*. Springer Verlag, 2009.

[7] J. Voelcker, "Lithium batteries take to the road," *Spectrum, IEEE*, vol. 44, pp. 26–31, 2007.

[8] A. Manthiram and J. Goodenough, "Lithium insertion into fe2(so4)3 frameworks," *Journal of Power Sources*, vol. 26, pp. 403–408, 1989.

[9] A. Padhi, "Phospho olivines as positive electrode materials for rechargeable lithium batteries," *Journal of the Electrochemical Society*, vol. 144, p. 1188, 1997.

[10] S. Chung, "Electronically conductive phospho-olivines as lithium storage electrodes," *Nature materials*, vol. 1, pp. 123–128, 2002.

[11] V. Hyrman, "Ect: the search for the perfect stimulus," *Biological psychiatry*, vol. 20, pp. 634–645, 1985.

[12] Y. Xia, *Development of Low Cost Cathode Materials for Lithium-ion Batteries*. PhD thesis, Saga University, 2008.

[13] T. Nagaura and K. Tozawa, "Lithium-ion rechargeable batteryprogress in batteries and solar cells," *Progress in Batteries and Solar Cells*, vol. 9, pp. 209–217, 1990.

[14] K. Abe, "Functional electrolytes," *Journal of the Electrochemical Society*, vol. 154, p. A810, 2007.

[15] S. Zhang, "A review on electrolyte additives for lithium-ion batteries," *Journal of Power Sources*, vol. 162, pp. 1379–1394, 2006.

[16] K. Abe, "Additives-containing functional electrolytes for suppressing electrolyte decomposition in lithium-ion batteries," *Electrochimica Acta*, vol. 49, pp. 4613–4622, 2004.

[17] H. Yoshitake, "The effect of nano-sized sei film formed by vinyl acetate additive for li-ion batteries," *Chemistry Letters*, vol. 32, pp. 134–135, 2003.

[18] B. Ellis, "A multifunctional 3.5 v iron-based phosphate cathode for rechargeable batteries," *Nature materials*, vol. 6, pp. 749–753, 2007.

[19] H. Fu, *Implementations of electric vehicle system based on solar energy in Singapore assessment of lithium-ion batteries for automobiles*. Massachusetts Institute of Technology, 2009.

[20] J. Hong, "Vanadium modified lifepo[sub 4] cathode for li-ion batteries," *Electrochemical and Solid-State Letters*, vol. 12, pp. A33–A38, 2009.

[21] B. Kumar, "A solid-state, rechargeable, long cycle life lithium-air battery," *Journal of the Electrochemical Society*, vol. 157, p. A50, 2010.

[22] K. Nam, "Virus-enabled synthesis and assembly of nanowires for lithium-ion battery electrodes," *Science*, vol. 312, p. 885, 2006.

[23] B. Kumar, "High-performance lithium battery anodes using silicon nanowires," *Nature nanotechnology*, vol. 3, pp. 31–35, 2007.

[24] S. Levy and P. Bro, *Battery hazards and accident prevention*. Springer, 1994.

[25] H. Choi, "A study of the mechanism of the electrochemical reaction of lithium with coo by two-dimensional soft x-ray absorption spectroscopy (2d xas), 2d raman, and 2d heterospectral xas- raman correlation analysis," *J. Phys. Chem. B*, vol. 107, pp. 5806–5811, 2003.

[26] G. G. Amatucci, "Coo[sub 2], the end member of the li[sub x]coo[sub 2] solid solution," *Journal of the Electrochemical Society*, vol. 143, pp. 1114–1123, 1996.

[27] V. Johnson, *Temperature-dependent battery models for high-power lithium-ion batteries*. National Renewable Energy Laboratory, 2001.

[28] P. Balakrishnan, "Safety mechanisms in lithium-ion batteries," *Journal of the Electrochemical Society*, vol. 155, pp. 401–414, 2006.

[29] G. Venugopal, "Characterization of thermal cut-off mechanisms in prismatic lithium-ion batteries," *Journal of Power Sources*, vol. 101, pp. 231–237, 2001.

[30] F. Laman, "Impedance studies for separators in rechargeable lithium batteries," *Journal of the Electrochemical Society*, vol. 140, p. L51, 1993.

[31] K. Xu, "Nonflammable electrolytes for li-ion batteries based on a fluorinated phosphate," *Journal of the Electrochemical Society*, vol. 149, p. A1079, 2002.

[32] D. Lee, "Redox shuttle additives for chemical overcharge protection in lithium-ion batteries," *Korean Journal of Chemical Engineering*, vol. 19, pp. 645–652, 2002.

[33] S. Sloop, "Chemical reactivity of pf and lipf in ethylene carbonate/dimethyl carbonate solutions," *Electrochemical and Solid-State Letters*, vol. 4, p. A42, 2001.

[34] E. Zinigrad, "On the thermal stability of lipf6," *Thermochimica Acta*, vol. 438, pp. 184–191, 2005.

[35] D. Aurbach, "On the use of vinylene carbonate (vc) as an additive to electrolyte solutions for li-ion batteries," *Thermochimica Acta*, vol. 47, pp. 1423–1439, 2002.

[36] D. Ilic, "Poliflex (tm), the innovative lithium-polymer battery," *Journal of Power Sources*, vol. 129, pp. 34–37, 2004.

[37] C. J. Mikolajczak, "A scientific methodology for investigation of a lithium-ion battery failure," in *Portable Information Devices*, vol. PORTABLE07, pp. 1–6, IEEE International Conference on Applications and Advances, 2007.

[38] J. Loud, "On the testing methods of simulating a cell internal short circuit for lithium-ion batteries," in *Battery Conference on Applications and Advances*, vol. The Seventeenth Annual, pp. 205–208, 2002.

[39] U. Troltzsch, "Characterizing aging effects of lithium-ion batteries by impedance spectroscopy," *Electrochimica Acta*, vol. 51, pp. 1664–1672, 2006.

[40] S. Komagata, "Detection of degradation of lithium-ion batteries with acoustic emission technique," *ECS Meeting Abstracts*, vol. 902, p. 83, 2009.

[41] M. Isaacson, "Advanced lithium ion battery charger," pp. 193 – 198, Battery Conference on Applications and Advances, 2000. The Fifteenth Annual, 2000.

[42] Y. Saito, "Thermal studies of a lithium-ion battery," *Journal of Power Sources*, vol. 68, pp. 451–454, 1997.

[43] J. Gnanaraj, "The use of accelerating rate calorimetry (arc) for the study of the thermal reactions of li-ion battery electrolyte solutions," *Journal of Power Sources*, vol. 119, pp. 794–798, 2003.

[44] V. Pop, *Battery management systems: accurate state-of-charge indication for battery powered applications*. Springer Verlag, 2008.

[45] S. Lee, "The state and parameter estimation of an li-ion battery using a new ocv-soc concept," pp. 2799–2803, Power Electronics Specialists Conference, 2007. PESC 2007. IEEE, 2007.

[46] H. Bergveld, *Battery management systems: design by modelling*. Kluwer Academic Publishers, 2002.

[47] F. Huet, "A review of impedance measurements for determination of the state-of-charge or state-of-health of secondary batteries," *Journal of Power Sources*, vol. 70, pp. 59–69, 1998.

[48] K. E. Thomas and J. Newman, "Thermal modeling of porous insertion electrodes," *Journal of the Electrochemical Society*, vol. 150, pp. A176–A192, 2003.

[49] N. Sato, "Thermal behavior analysis of lithium-ion batteries for electric and hybrid vehicles," *Journal of Power Sources*, vol. 99, pp. 70–77, 2001.

[50] K. Kumaresan, "Thermal model for a li-ion cell," *Journal of the Electrochemical Society*, vol. 155, pp. A164–A171, 2008.

[51] W. M. Deen, *Analysis of transport phenomena*. Oxford University Press, New York, 1998.

APPENDIX

APPENDIX: SIMPLIFIED LOOKUP TABLES OF HEATING POWER

Table A.1
Lookup table of heating power of discharging in normal condition

Current Rate	-1	-0.9	-0.8	-0.7	-0.6	-0.5
100	-0.24469	0.048517	-1.35666	0.055352	-0.51739	0.022639
99	0.071557	0.069561	-0.42596	0.015665	-0.15968	0.013033
98	0.135348	0.092048	-0.22638	0.003788	-0.09467	0.006696
97	0.227481	0.111609	0.054967	-0.01154	0.015238	-0.00063
96	0.186048	0.121179	0.036649	0.000802	-0.01793	-0.00879
95	0.181613	0.130227	0.067757	0.000645	0.003621	-0.02828
94	0.134282	0.129208	0.07099	0.023904	-0.00609	-0.04024
93	0.113645	0.127931	0.077926	0.031915	0.00733	-0.04173
92	0.082032	0.123299	0.089695	0.054073	0.006973	-0.04387
91	0.068319	0.124362	0.093778	0.065321	0.021324	-0.03576
90	0.056055	0.125179	0.101001	0.078768	0.03257	-0.01449
89	0.051691	0.127018	0.10047	0.085158	0.045753	0.003225
88	0.05424	0.128105	0.10384	0.090882	0.057237	0.012511
87	0.058204	0.128611	0.103753	0.093563	0.065863	0.023989
86	0.071829	0.126995	0.106746	0.099653	0.071553	0.043277
85	0.089206	0.125128	0.108954	0.106149	0.072764	0.056818
84	0.109257	0.124879	0.111552	0.107381	0.073613	0.057982
83	0.12477	0.124207	0.116575	0.107334	0.074294	0.062252

82	0.139795	0.123823	0.119973	0.106958	0.074001	0.06599
81	0.148467	0.12281	0.119728	0.102625	0.073287	0.054461
80	0.151155	0.119738	0.117783	0.098599	0.06938	0.048586
79	0.151732	0.114978	0.114822	0.099106	0.064927	0.05147
78	0.15559	0.110661	0.111071	0.100162	0.061211	0.050105
87	0.058204	0.128611	0.103753	0.093563	0.065863	0.023989
86	0.071829	0.126995	0.106746	0.099653	0.071553	0.043277
85	0.089206	0.125128	0.108954	0.106149	0.072764	0.056818
84	0.109257	0.124879	0.111552	0.107381	0.073613	0.057982
83	0.12477	0.124207	0.116575	0.107334	0.074294	0.062252
82	0.139795	0.123823	0.119973	0.106958	0.074001	0.06599
81	0.148467	0.12281	0.119728	0.102625	0.073287	0.054461
80	0.151155	0.119738	0.117783	0.098599	0.06938	0.048586
79	0.151732	0.114978	0.114822	0.099106	0.064927	0.05147
78	0.15559	0.110661	0.111071	0.100162	0.061211	0.050105
77	0.158705	0.109546	0.107595	0.099855	0.060321	0.039545
76	0.159311	0.10939	0.105985	0.099154	0.060272	0.031392
75	0.160906	0.112226	0.105938	0.099019	0.062784	0.028587
74	0.162298	0.115514	0.105516	0.098283	0.065491	0.027447
73	0.16354	0.117372	0.103893	0.097439	0.065284	0.026675
72	0.162614	0.117415	0.102691	0.09839	0.064475	0.035278
71	0.162085	0.11651	0.102365	0.099545	0.064063	0.043189
70	0.162293	0.117019	0.101928	0.099951	0.062929	0.043977
69	0.156615	0.11663	0.103138	0.099978	0.069616	0.04138
68	0.147471	0.117524	0.102442	0.099726	0.079858	0.055773
67	0.139905	0.11898	0.099642	0.098393	0.07932	0.069963
66	0.137969	0.119953	0.098035	0.097344	0.078302	0.067475
65	0.137214	0.120189	0.097755	0.096974	0.081193	0.070038
64	0.140912	0.120029	0.097848	0.096795	0.07541	0.075908
63	0.149013	0.121186	0.099669	0.097069	0.067669	0.064155
62	0.15582	0.130363	0.103388	0.098655	0.069925	0.053632

61	0.157884	0.144303	0.106344	0.10122	0.071946	0.057671
60	0.15876	0.157872	0.110229	0.096024	0.071207	0.057652
59	0.161836	0.164639	0.111899	0.084064	0.071287	0.056873
58	0.164677	0.168135	0.11318	0.078583	0.075931	0.058739
57	0.167609	0.164266	0.116823	0.077774	0.082939	0.060042
56	0.169728	0.157319	0.120562	0.076755	0.084981	0.060625
55	0.171665	0.151798	0.120303	0.085086	0.088382	0.063116
54	0.172428	0.152579	0.12061	0.098915	0.092112	0.06593
53	0.172667	0.156047	0.123868	0.105527	0.0914	0.066528
52	0.173362	0.155784	0.125962	0.107478	0.087635	0.06724
51	0.175308	0.156833	0.127766	0.109478	0.087319	0.071417
50	0.177624	0.156716	0.132216	0.110362	0.091065	0.069062
49	0.18033	0.159592	0.135872	0.112714	0.092923	0.065091
48	0.183154	0.163721	0.136839	0.114826	0.093785	0.06785
47	0.186792	0.171193	0.138277	0.120878	0.090648	0.069642
46	0.191389	0.17758	0.141129	0.137167	0.086811	0.06867
45	0.194954	0.182361	0.143646	0.151755	0.085837	0.072415
44	0.197893	0.183335	0.147689	0.157501	0.085487	0.080163
43	0.201318	0.183761	0.152808	0.16323	0.086507	0.078521
42	0.205198	0.183174	0.15477	0.164441	0.094322	0.080334
41	0.208911	0.183732	0.156574	0.155728	0.103881	0.080367
40	0.212913	0.186043	0.1603	0.14895	0.106095	0.07469
39	0.217167	0.192856	0.163718	0.150596	0.10928	0.075934
38	0.218851	0.201639	0.165644	0.15443	0.111769	0.079483
37	0.219167	0.208679	0.169997	0.159001	0.113749	0.079715
36	0.221677	0.214279	0.173682	0.162698	0.117701	0.083819
35	0.227983	0.219326	0.174965	0.166381	0.122063	0.093698
34	0.236511	0.223949	0.177666	0.17029	0.126161	0.09709
33	0.244795	0.225774	0.183569	0.168141	0.129134	0.098564
32	0.25268	0.229458	0.189115	0.16283	0.131358	0.107631

31	0.257959	0.233041	0.193655	0.163025	0.133488	0.123415
30	0.261182	0.235709	0.199247	0.166726	0.136185	0.128974
29	0.262789	0.236906	0.203273	0.169453	0.13844	0.130522
28	0.265365	0.239607	0.204407	0.177368	0.141987	0.136773
27	0.269753	0.243712	0.206464	0.186696	0.146312	0.135317
26	0.275208	0.24627	0.209393	0.189063	0.148846	0.125425
25	0.279843	0.247695	0.211066	0.18919	0.148217	0.124735
24	0.28442	0.249079	0.212988	0.190044	0.145412	0.126853
23	0.288396	0.248668	0.215483	0.190035	0.144825	0.122449
22	0.290438	0.245598	0.215392	0.191472	0.144294	0.11187
21	0.290245	0.243279	0.212874	0.190649	0.142102	0.110399
20	0.289825	0.242604	0.208579	0.192183	0.142782	0.110012
19	0.290518	0.240366	0.203597	0.199854	0.145754	0.106181
18	0.290308	0.238636	0.201301	0.202673	0.143638	0.106834
17	0.28948	0.235474	0.200209	0.198589	0.138719	0.113392
16	0.287129	0.23266	0.198938	0.19712	0.135986	0.11055
15	0.283849	0.227175	0.198222	0.190496	0.131544	0.107091
14	0.278547	0.220503	0.194843	0.177753	0.128087	0.103546
13	0.273181	0.213301	0.187763	0.170407	0.130013	0.097541
12	0.267727	0.206082	0.180751	0.166557	0.129334	0.093632
11	0.263208	0.203051	0.17576	0.160024	0.12539	0.090451
10	0.259751	0.202829	0.170684	0.158051	0.123125	0.085865
9	0.257246	0.207074	0.167704	0.157947	0.121253	0.084849
8	0.256339	0.212665	0.166794	0.156816	0.117079	0.08663
7	0.256277	0.221728	0.166542	0.156938	0.116662	0.08697
6	0.259813	0.230175	0.16852	0.155861	0.120878	0.091097
5	0.26602	0.238662	0.179907	0.154984	0.126601	0.096722
4	0.272943	0.245598	0.197206	0.15891	0.132519	0.099373
3	0.279849	0.254397	0.213633	0.164154	0.138095	0.101613
2	0.290201	0.254523	0.229372	0.175614	0.146304	0.104038
1	0.292081	0.254523	0.248565	0.18929	0.150485	0.102002

Table A.2
Lookup table of heating power of charge in normal condition

Current Rate	0.5	0.6	0.7	0.8	0.9	1.0
100	0.006388	-0.00927	-0.0121	-0.05551	0.010477	-0.02218
99	-0.01822	-0.00144	0.002936	-0.02288	0.006493	0.008627
98	-0.01958	-0.00267	0.008618	-0.01282	0.00652	0.001007
97	-0.02132	-0.00185	0.010285	-0.00142	0.007516	0.015031
96	-0.01559	-0.00428	0.021617	0.001325	0.012232	0.018432
95	-0.00865	-0.00117	0.021901	0.007636	0.015951	0.021881
94	-0.00743	-0.00163	0.020353	0.011065	0.019026	0.019474
93	-0.00849	-0.00236	0.006797	0.012393	0.019644	0.010233
92	-0.01588	-0.00602	0.001044	0.012315	0.016608	0.002973
91	-0.02321	-0.01605	-0.01405	0.007863	0.009878	-0.00718
90	-0.03604	-0.02768	-0.03086	-0.01389	0.002452	-0.01402
89	-0.04448	-0.03793	-0.03798	-0.044	-0.00632	-0.02268
88	-0.05046	-0.04701	-0.04043	-0.06732	-0.01641	-0.02906
87	-0.05578	-0.05381	-0.04411	-0.07947	-0.02612	-0.03653
86	-0.05521	-0.05622	-0.04655	-0.09043	-0.03389	-0.04261
85	-0.0533	-0.05777	-0.04662	-0.08723	-0.0409	-0.04679
84	-0.0548	-0.05982	-0.0454	-0.07583	-0.04712	-0.05014
83	-0.05421	-0.06079	-0.04778	-0.06855	-0.04992	-0.04957
82	-0.05385	-0.06135	-0.05038	-0.06997	-0.04888	-0.05244
81	-0.05785	-0.06188	-0.04808	-0.07031	-0.04863	-0.05557
80	-0.05934	-0.06083	-0.04508	-0.07084	-0.04898	-0.05878
79	-0.0575	-0.06012	-0.04299	-0.06993	-0.0468	-0.05976
78	-0.05818	-0.05836	-0.03757	-0.06969	-0.04326	-0.05909
77	-0.06698	-0.05674	-0.03198	-0.06801	-0.04216	-0.05495

76	-0.07147	-0.0556	-0.02937	-0.06515	-0.04092	-0.0469
75	-0.07161	-0.05227	-0.0264	-0.05851	-0.03882	-0.03957
74	-0.07212	-0.04908	-0.02203	-0.04749	-0.03559	-0.03112
73	-0.06986	-0.04791	-0.01773	-0.03498	-0.03233	-0.0269
72	-0.05746	-0.04424	-0.01347	-0.02839	-0.02792	-0.02338
71	-0.04972	-0.03922	-0.01025	-0.02394	-0.02229	-0.01985
70	-0.04689	-0.03821	-0.0021	-0.02187	-0.01747	-0.015
69	-0.04118	-0.03279	0.007619	-0.02451	-0.01229	-0.01011
68	-0.03488	-0.025	0.012597	-0.02661	-0.00773	-0.00507
67	-0.03084	-0.02031	0.01753	-0.02391	-0.00338	0.001311
66	-0.0277	-0.01889	0.022461	-0.02004	0.001463	0.005288
65	-0.02474	-0.01613	0.021674	-0.01713	0.006211	0.011563
64	-0.02342	-0.01349	0.019675	-0.01301	0.010082	0.015449
63	-0.02369	-0.01413	0.02263	-0.00925	0.012517	0.020994
62	-0.02194	-0.01253	0.025607	-0.00569	0.014704	0.026292
61	-0.01956	-0.00747	0.028159	-0.00106	0.019358	0.022979
60	-0.01517	-0.00428	0.030256	0.004712	0.024896	0.016145
59	-0.00791	-0.00304	0.032	0.006592	0.029852	0.0089
58	-0.00275	0.004704	0.035016	0.006391	0.035116	0.005099
57	-0.00085	0.008765	0.031534	0.007522	0.04085	0.00776
56	0.00273	0.007395	0.023234	0.010298	0.043786	0.017057
55	0.003275	0.01195	0.02169	0.011877	0.045594	0.027384
54	-0.00084	0.01496	0.024334	0.015009	0.047054	0.038994
53	-0.00127	0.009971	0.024273	0.018937	0.04539	0.046014
52	0.001184	0.00862	0.029157	0.022649	0.041152	0.046335
51	-0.00049	0.013449	0.040736	0.024515	0.037156	0.050521
50	-0.00892	0.013744	0.045904	0.02579	0.036543	0.053493
49	-0.01093	0.015953	0.043795	0.026948	0.037093	0.055508

48	-0.01101	0.016722	0.044544	0.028573	0.042751	0.057382
47	-0.01205	0.008091	0.048476	0.029866	0.050299	0.056899
46	-0.00927	0.0024	0.04828	0.031822	0.056526	0.056308
45	0.000315	0.002769	0.047603	0.033581	0.05971	0.057754
44	0.00555	0.000321	0.05382	0.042254	0.061318	0.059473
43	0.004727	0.002641	0.060407	0.056471	0.060813	0.063855
42	0.008819	0.012105	0.062542	0.06716	0.060555	0.066964
41	0.019343	0.017883	0.064567	0.068701	0.0625	0.069467
40	0.022122	0.018908	0.066826	0.069926	0.06477	0.07883
39	0.021253	0.019411	0.065522	0.066963	0.066757	0.088685
38	0.024409	0.018627	0.061299	0.058721	0.067414	0.098457
37	0.021994	0.021132	0.059578	0.052213	0.068752	0.104933
36	0.013065	0.026947	0.06058	0.052276	0.065488	0.108125
35	0.011347	0.030425	0.060754	0.054694	0.060581	0.105124
34	0.010702	0.033683	0.05998	0.055914	0.056571	0.099662
33	0.006937	0.03385	0.060008	0.055993	0.056001	0.091703
32	-0.00034	0.032052	0.05979	0.057119	0.056471	0.088059
31	-0.00497	0.026554	0.055411	0.060073	0.059012	0.089268
30	-0.00667	0.021526	0.048681	0.061793	0.064016	0.089289
29	-0.00751	0.02073	0.045852	0.059886	0.069267	0.09146
28	-0.00561	0.021408	0.045778	0.057253	0.07236	0.092048
27	0.000727	0.021349	0.044132	0.054952	0.073759	0.093797
26	0.00337	0.019971	0.046802	0.053839	0.075282	0.093885
25	0.001791	0.018116	0.054957	0.052801	0.075361	0.094185
24	0.007708	0.01644	0.058231	0.053617	0.073381	0.093961
23	0.018293	0.017172	0.056106	0.055793	0.07167	0.095303
22	0.021142	0.017167	0.055989	0.055608	0.070703	0.098341
21	0.023429	0.017578	0.058204	0.054147	0.071418	0.10009

20	0.028137	0.020015	0.059981	0.053993	0.072547	0.105129
19	0.025484	0.021991	0.063646	0.056665	0.073225	0.112173
18	0.020019	0.024028	0.062425	0.058115	0.080455	0.120858
17	0.025403	0.027205	0.055147	0.060764	0.091401	0.128498
16	0.031409	0.034612	0.054542	0.063586	0.102287	0.13204
15	0.038759	0.035319	0.058254	0.066604	0.107574	0.130698
14	0.047547	0.027463	0.060868	0.069747	0.111351	0.125708
13	0.055075	0.028601	0.07505	0.070171	0.11126	0.121101
12	0.062358	0.034674	0.095428	0.068359	0.107433	0.118451
11	0.06889	0.038909	0.106021	0.069819	0.104106	0.121779
10	0.073621	0.050795	0.110984	0.075104	0.106435	0.127049
9	0.076633	0.068295	0.116274	0.079762	0.112781	0.132561
8	0.074784	0.077174	0.118492	0.089092	0.117541	0.136543
7	0.068657	0.080478	0.117283	0.102004	0.12189	0.139386
6	0.056922	0.076852	0.113129	0.112836	0.125735	0.14131
5	0.041059	0.069051	0.108267	0.119862	0.1324	0.142435
4	0.025664	0.074945	0.099531	0.125059	0.139652	0.145577
3	0.013059	0.088674	0.093743	0.129313	0.145928	0.147711
2	0.002174	0.103516	0.108267	0.133783	0.15488	0.148568
1	-0.00283	0.138371	0.099531	0.136734	0.15766	0.145577